

Development and Characterization of a Microfluidic Method for Real-Time Generation of
Transiently Stable Biocompatible Microbubbles *In Situ* for Image-Guided Therapy

A Thesis

Presented to

the faculty of the School of Engineering and Applied Science

University of Virginia

in partial fulfillment of the
requirements for the degree

Master of Science

By

Johnny L Chen

May

2013

APPROVAL SHEET

The thesis
is submitted in partial fulfillment of the requirements
for the degree of
Master of Science



AUTHOR


The thesis has been read and approved by the examining committee:

John A. Hossack
Advisor

Alexander L. Klibanov

Richard J. Price

Accepted for the School of Engineering and Applied Science:



Dean, School of Engineering and Applied Science

May

2013

Acknowledgements

This work would not have been possible without the contribution of numerous professors, students, friends, and family. I would like to thank my advisor, Dr. John Hossack, for his persistent faith in me and for supporting and guiding my research all these years. Without his dedication, my work would not have fostered and grown to its fullest extent. Additionally, I would like to thank Dr. Alexander Klibanov for his insight and support on my project as well as the open access to his lab and equipment. His discussions led to many great ideas and motivations.

I would like to thank the Price, French, and Lawrence lab for access to their equipment. In addition, I thank Dr. Arthur Lichtenberger for assistance with photolithography and Dr. David Green for discussions on viscometry. I thank all lab members, past and present, for their input, support, and encouragement: Ali Dhanaliwala, Adam Dixon, Shiyang Wang, Joseph Kilroy, Will Mauldin, Kevin Owens, Linsey Phillips, Abhay Patil, Matt Hudson, Dan Lin, and Bryce Lowrey. I would like to acknowledge Brian Shin, an undergraduate research assistant for help with experiments and image processing.

I would like to thank Springer for permission to use the content and figures in chapter 2, which was originally published in *Microfluidics Nanofluidics*. The content in chapter 3 was recently submitted to Elsevier *Ultrasound in Medicine & Biology*.

Lastly, I would like to thank my family for their support and letting me follow my passion. I will always be grateful for the opportunities they worked so hard to provide me with.

Sources of funding included National Institute of Health grant NHLBI R01 HL090700 and a shared instrumentation grant S10 RR025594. Bovine blood was also provided by Gore Processing Inc.

Table of Contents

Abstract	VII
List of Symbols and Abbreviations	VIII
List of Figures	X
List of Tables	XII
Chapter 1 Introduction	1
1.1 Microbubbles	1
1.2 Microbubble Shells	2
1.2.1 Protein	4
1.2.2 Lipid	4
1.2.3 Polymer	5
1.2.4 Surface Modification and Drug Loading	5
1.3 Controlling Size Distribution	7
1.4 Microfluidics	9
1.4.1 Microfluidic Generation of Microbubbles	9
1.4.2 Microfluidic Interconnects	11
1.5 Specific Aims	12
Chapter 2 Fabrication and Characterization of a Flooded Microfluidic Catheter Prototype for <i>In Situ</i> Microbubble Generation	13
2.1 Introduction	13
2.2 Materials and Methods	16
2.2.1 Microfluidic Device Fabrication	16
2.2.2 Microbubble Formulation	19
2.2.3 Microbubble Production	19
2.3 Results and Discussion	20
2.3.1 FFMD Fabrication	20
2.3.2 Microbubble Production and Characterization	20

2.4 Conclusions	24
Chapter 3 Synthesis and Characterization of Transiently Stable Albumin-Coated Microbubbles.....	26
3.1 Introduction	26
3.2 Materials and Methods	28
3.2.1 FFMD Fabrication.....	28
3.2.2 Microbubble Fabrication.....	29
3.2.3 Microbubble Characterization.....	29
3.2.3 Microbubble Characterization.....	30
3.2.5 Plasma Microbubbles	33
3.2.6 Statistical Analysis	34
3.3 Results and Discussion.....	35
3.3.1 BSA Microbubble Coalescence	35
3.3.2 BSA Microbubble Stability.....	37
3.3.3 Calcein Delivery.....	39
3.3.4 Bovine Plasma Microbubbles	41
3.4 Conclusions	43
Chapter 4 Discussion and Conclusions	45
Appendix Microbubble Detection Algorithm	47
References	52

Abstract

Microbubbles are ultrasound contrast and therapeutic agents with a gas core encapsulated by a shell. Conventional methods of production (i.e. agitation and sonication) result in a polydisperse distribution that must be size-sorted before administration. With systemic administration by IV or bolus injection, microbubbles experience changes in diameter, distribution, and concentration during transit in the vasculature, resulting in unknown microbubble characteristics at the site of interest. We report a microfluidic method of generating monodisperse microbubbles *in situ*, to eliminate the uncertainty in microbubble characteristics *in vivo*. We introduce a novel method of supplying the shell and gas material to a flow-focusing microfluidic device (FFMD), enabling FFMDs to be potentially scaled down to vascular dimensions. By producing microbubbles in real-time *in situ*, novel microbubble compositions are possible, such as larger microbubbles for increased contrast and bioeffects. Additionally, microbubbles with semi-stable shells can be utilized to facilitate rapid dissolution downstream the site of interest, reducing the risk of gas entrapment in small vessels. We demonstrate that real-time production of transiently stable microbubbles upstream can improve image contrast and delivery of a model drug under flow. Lastly, we show that a completely biocompatible microbubble can be generated with a microfluidic device from whole blood. This demonstrates the potential for a lab-on-a-chip method of generating an image-guided therapeutic agent at the point-of-care using a patient's own blood as the medium.

List of Symbols and Abbreviations

AAL	Acoustically active liposphere
BSA	Bovine serum albumin
CPS	Contrast pulse sequences
FFMD	Flow-focusing microfluidic device
eFFMD	Externally mounted flow-focusing microfluidic device
iFFMD	Internally mounted flow-focusing microfluidic device
PEG40S	Polyethylene glycol-40-stearate
GPS	Glycerol and propylene glycol in saline
HSA	Human serum albumin
IVUS	Intravascular ultrasound
MI	Mechanical index
MB	Microbubble
PDI	Polydispersity index
PDMS	Polydimethylsiloxane
PI	Propidium iodide
PMMA	Poly(methyl methacrylate)
PNP	Peak negative pressure
PRF	Pulse repetition frequency
PTFE	Polytetrafluoroethylene
Si	Silicon
SMC	Smooth muscle cells
ΔP	Pressure difference between inside and outside of microbubble
γ	Surface tension
R	Microbubble radius
P	Pressure inside microbubble
k	Henry's constant

C	Concentration of gas in solute
η	Viscosity
T_i	Time until half the maximum image intensity
T_{mb}	Time until half the maximum number of microbubbles
μ_d	Mean diameter
σ_d	Standard deviation of diameter

List of Figures

Chapter 1

Figure 1.1 Schematic of common microbubble shells	3
Figure 1.2 Schematic of drug loading strategies	6
Figure 1.3 Schematic of FFMD microbubble production	10
Figure 1.4 Schematic of interconnects	11

Chapter 2

Figure 2.1 Schematic of flooded catheter	15
Figure 2.2 Photolithography steps	17
Figure 2.3 Schematic of FFMD mold	18
Figure 2.4 Schematic of non-flooded and flooded FFMDs	18
Figure 2.5 Production regimes in a FFMD	21
Figure 2.6 Production curve of a FFMD	22
Figure 2.7 Polydispersity of FFMD	23

Chapter 3

Figure 3.1 Schematic of flow chamber setup	31
Figure 3.2 Effect of dextrose and glycerol + propylene glycol on coalescence	34
Figure 3.3 Optical determination of half-life	36
Figure 3.4 Acoustic determination of half-life	37
Figure 3.5 Calcein delivery	39
Figure 3.6 Bovine plasma imaging	41

Chapter 4

Figure 4.1 Microfluidics IVUS catheter.....	45
---	----

Appendix

Figure A.1 Microbubble images	47
-------------------------------------	----

Figure A.2 Flow diagram for microbubble detection	48
---	----

Figure A.3 Microbubbles detected with CHT	49
---	----

List of Tables

Chapter 2

Table 2.1 Production from flooded FFMDs	24
---	----

Chapter 1

Introduction

1.1 Microbubbles

Microbubbles are gas filled particles that have been investigated for a wide range of applications, such as the production of foams in the food and beverage industry to enhance appearance or texture [1]. Microbubbles are also effective cleaning or purifying agents, having been used for cleaning oil on mechanical parts or biofilms on teeth [2] as well as purifying contaminated water [3]. There has been extensive research on the medical benefits of microbubbles, specifically for use as ultrasound contrast agents.

Several contrast agents exist for other imaging modalities, namely iodine or barium for x-ray and computed tomography (CT) and gadolinium for magnetic resonance (MR). Iodine- or barium-based agents work by attenuating ionizing radiation. Gadolinium-based agents work altering the magnetization properties of surrounding molecules. Microbubble agents effectively scatter ultrasound energy. The density of the gas core is lower than that of the surrounding blood and tissues, creating an interface that causes a large backscatter or echo when excited with ultrasonic energy. The general application of these contrast agents is to highlight certain structures in the body non-invasively.

Microbubbles are about the size of red blood cells ($< 10\mu\text{m}$), and thus exhibit similar rheological properties, making them useful for assessing blood flow and perfusion in organs. Microbubbles were first used for contrast echocardiography, where the contrast was provided by hand-agitated solutions of saline. That has since evolved into more sophisticated pharma-

ceutical and in-house preparations for various applications. Microbubbles are used for the detection of cardiac wall motion abnormalities [4], molecular targeting and imaging [5], drug delivery [6], sonothrombolysis [7], and many other applications.

1.2 Microbubble Shells

One limitation of microbubbles is their stability. The gaseous core readily diffuses when exposed to a concentration or pressure gradient. Microbubbles are subject to high Laplace pressure, an inward force that is a consequence of the surface tension of the liquid-gas interface. The Laplace pressure is defined as

$$\Delta P = \frac{2\gamma}{R} \quad (1)$$

where ΔP is the pressure difference between the inside and outside of the microbubble, γ is the surface tension, and R is the radius of the microbubble. Smaller microbubbles have a higher Laplace pressure that will contribute to gas diffusion out—like a “squeezing” effect—of the microbubble and into the surrounding media, as dictated by Henry’s law:

$$P = kC \quad (2)$$

Where P is the pressure inside the microbubble, k is the Henry constant describing solubility of the gas, and C is the concentration of gas in the surrounding media. The Laplace pressure contributes to Ostwald ripening [8] of microbubbles, where microbubbles within close proximity exchange gases with each other. Larger particles are more thermodynamically stable than smaller particles so large microbubbles tend to grow by drawing gas from smaller microbubbles, causing smaller microbubbles to shrink and potentially collapse.

Another factor that affects microbubble stability is microbubble coalescence, the fusion of multiple microbubbles to form a larger microbubble. Coalescence occurs when the

thin film between touching microbubbles break, leading to a larger microbubble with lower surface tension as determined by equation (1). Desire for more stable microbubble dispersions in order to increase microbubble contrast duration has prompted the development of stabilizing shells to prevent gas diffusion and microbubble coalescence.

Typical microbubble shells are a few nanometers to several hundred nanometers thick depending on the type of shell (e.g. lipid, protein, or polymer) (Fig.1.1). Amphiphilic molecules are popular shell materials as they consist of a hydrophobic and hydrophilic moiety, allowing for organized arrangement into monolayers to form microbubbles. They act as surfactants to lower the surface tension, and thus the Laplace pressure. In conjunction with a shell, an insoluble gas, such as a perfluorocarbon or sulfur hexafluoride, is often used to prevent microbubble diffusion. Shell-stabilized microbubbles have been shown to have excellent shelf life, remaining stable for over a year.

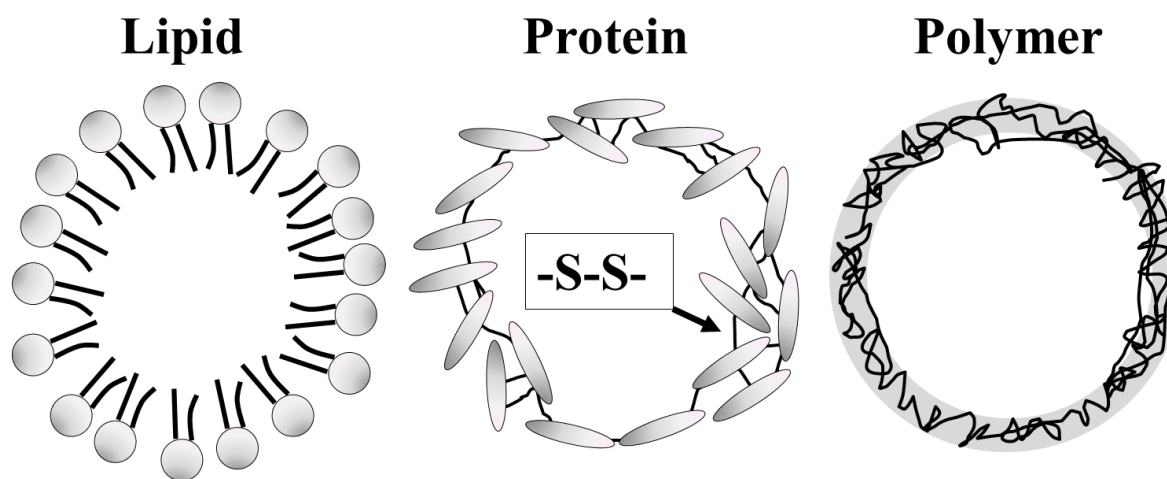


Figure 1.1: Schematic of common microbubble shells. The core is filled with a gas such as nitrogen, perfluorocarbon, or sulfur hexafluoride. Lipid shells arrange in a monolayer formation, with hydrophilic headgroups facing the aqueous phase. Protein shells are held together by single to multi-layered proteins cross-linked by disulfide bridges between cysteine residues. Polymer shells are comprised of heavily cross-linked or entangled monomers. Not drawn to scale.

1.2.1 Protein

The first generation of approved microbubbles in the US was made from sonicated human albumin. The first formulation approved by the US Food and Drug Administration (FDA) was Albunex (GE Healthcare), made from sonicated 5% human serum albumin in the presence of air. The shell thickness was found to be approximately 15 nm comprised of denatured cross-linked albumin molecules in different orientations [9]. Disulfide bonds between cysteine residues are formed during sonication, producing a rigid shell [10].

Other proteins have also been used to form microbubbles, given the amphiphilic nature of many proteins. Heating is typically needed to denature the proteins and simple emulsification, such as by vortex mixing, is not sufficient to form stable long lasting microbubbles. Wong and Suslick have demonstrated the formation of microspheres using hemoglobin as a potential blood substitute [11].

1.2.2 Lipid

There are several commercially available lipid-stabilized microbubbles in the US, one of them being Definity (Lantheus Medical Imaging), an octafluoropropane based contrast agent. Phospholipids self-assemble with their hydrophobic tails oriented inward towards the gas and their hydrophilic head group outward towards the aqueous phase. Phospholipids produce excellent microbubbles because the monolayer can compress to a solid-like condensed phase with near zero surface tension. Phospholipids also do not require any cross-linking, and thus can be easily formed using various methods other than sonication [12]. Lipid monolayers are also more compliant than protein monolayers, allowing more expansion and compression compared to similar protein microbubbles [13].

1.2.3 Polymer

Microbubbles fabricated from polymers are more resistant to microbubble expansion or compression due to the bulk cross-linking or entanglement of the monomers. Thus, their echogenicity may be compromised and their shell may fracture, leading to release of an unshelled gaseous core [14]. Microbubbles have been fabricated from various polymers, such as poly vinyl alcohol (PVA) and poly-D,L-lactide-co-glycolide (PLGA). One method of generating polymer microbubbles is by formation of a closed microsphere and subsequent removal (e.g. by sublimation) [15]. Polymer microbubbles exhibit excellent stability and can also carry various drugs and ligands.

1.2.4 Surface Modifications and Drug Loading

Extensive preclinical work has been done on modifying microbubbles for molecular targeting and drug delivery. Ligands targeted to receptors on endothelia have been conjugated to microbubbles for various pathologies. For example, microbubbles have been targeted to investigate inflammatory markers in the vasculature such as E- and P-selectin [16]. A significant amount of surface modifications, however, has been performed with streptavidin-biotin molecules and thus are not directly translatable to humans.

Utilization of microbubbles as drug delivery vehicles has been demonstrated by many research groups. Drugs can be loaded by several methods, such as within the shell in the same monolayer plane or attached to the outside of the microbubble via electrostatic interactions or covalent bonds. For proteins, their negative charge inhibits attachment of nucleic acids. One strategy is to trap plasmid DNA within the cross-linked shell matrix. One disadvantage of the

microbubble shell is that there is a small volume and surface area where the drug can be incorporated, thus dosage per microbubble is quite limited. Several loading strategies have been developed to increase the amount of drug per microbubble. Drug-loaded liposomes have been attached to microbubbles to form acoustically responsive complexes with increased drug carrying capacity (Fig 1.2) [17]. Using liposomes several times smaller than microbubbles significantly increases the surface area available for drug loading. Drugs have also been incorporated within a thick oil layer in microspheres called multi-layered microbubbles or acoustically active lipospheres (AAL) [18]. The outermost layer is typically phospholipid, followed by an intermediate thick oil layer, and a gas core (Fig 1.2). The oil layer can incorporate hydrophobic drugs such as paclitaxel and doxorubicin.

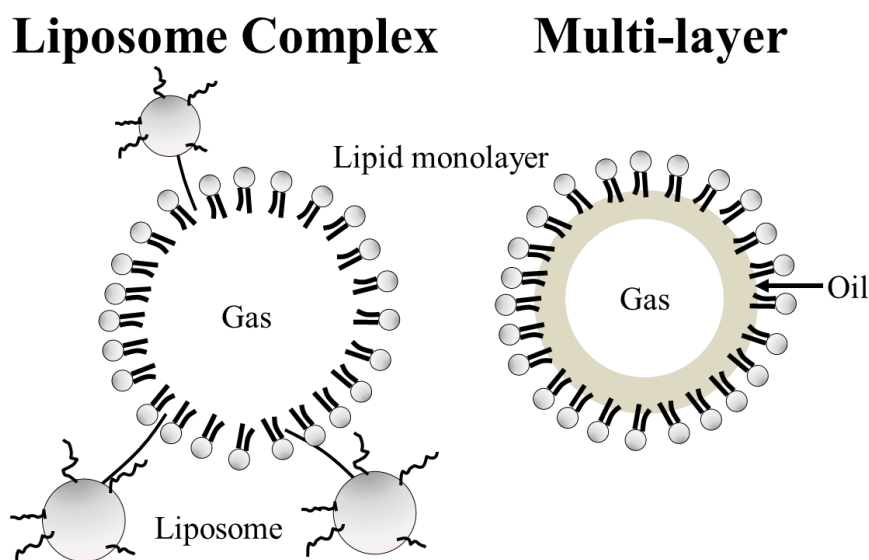


Figure 1.2: Schematic of a microbubble-liposome complex for improved drug loading. The microbubble is typically a few micrometers while liposomes are a few hundred nanometers. Multi-layered or acoustically active lipospheres are comprised of a lipid outer shell, a hydrophobic oil layer, and a gas core. Not drawn to scale.

1.3 Controlling Size Distribution

The most common method for microbubble production is agitation (i.e. shaking or sonication), in which a gas is dispersed within a liquid solution containing a shell material. Agitation methods can produce billions of microbubbles in a short amount of time; however, these populations usually have a wide size distribution with a polydispersity index as high as 150% [12]. The polydispersity index is defined as:

$$PDI = \frac{\sigma_d}{\mu_d} \times 100\% \quad (3)$$

Where μ_d is the mean microbubble diameter and σ_d is the standard deviation of microbubble diameter. Polydisperse populations are often size-sorted to obtain narrower size distributions. Floatation is one technique of microbubble separation [19]. In aqueous media, a buoyancy force is exerted on microbubbles because of their low density gas core and the force is proportional to their size—with larger microbubbles rising more quickly. Thus large microbubbles can be easily separated from smaller microbubbles by using differential rise times. Centrifugation is also an effective means of separating by microbubble size [20]. Although these methods are highly effective in narrowing the distribution, yield is reduced and specific diameters are difficult to isolate. Alternative methods such as size separation in flow chambers or filters have also been explored, but these methods generally require dilution and filters are easily clogged by larger microbubbles or particulates. Size-separation is a necessary procedure for most microbubble preparations, as different sized microbubbles have different acoustic signals and bioeffects. Monodisperse populations, typically $PDI < 10\%$, provide several benefits over polydisperse populations of microbubbles.

Microbubbles insonated at resonance produce maximal signal, which is of particular importance in cases where microbubble quantity is limited (e.g. molecular targeting and imaging). The resonant frequency—and subsequently the performance—of a microbubble is strongly dependent on its diameter. As the diameter increases, the resonant frequency decreases [21]. This dependence on size has prompted studies on monodisperse populations and their effect on imaging and drug delivery.

A monodisperse population of microbubbles insonated at their resonant frequency will scatter echoes more efficiently compared to a similar polydisperse microbubble population since a larger fraction of microbubbles will be oscillating at resonance. It has been shown for individual microbubbles improved correlation between echoes for a monodisperse population [22], [23]. Also, studies with microbubble suspensions have shown greater attenuation at the resonant frequency for monodisperse populations [24].

The advantages of monodispersity for therapeutic applications have not been investigated as extensively as for imaging applications. However, some preliminary results have shown the potential impact of monodispersity on therapy. Blood brain barrier (BBB) opening in mice has been shown to be dependent on microbubble size [25]. Also, selective ultrasonic sonoporation of single cells is dependent on microbubble size [26]. Although no study has clearly compared the therapeutic efficacy of monodisperse and polydisperse clouds of microbubbles with consistent mean diameters, preliminary results suggest that the microbubble size distribution can be matched to ultrasound settings for greater therapeutic effect. Instead of isolating a monodisperse population of microbubbles from a polydisperse population, an alternative is to directly generate microbubbles of uniform size. Microfluidic devices are ideal for such a task.

1.4 Microfluidics

Microfluidics involves the precise control of fluids, typically contained within a lab-on-a-chip system. Flow can be controlled by features such as pumps, valves and channels designed on the chip. The behavior of fluids at the microscale differs from its macroscale behavior in properties such as surface tension (i.e. capillary forces), viscosity, flow resistance, heating, and diffusion. Microfluidic chips have a small form factor enabling point-of-care without bulky equipment. Sample volumes typically range from picoliters to microliters, which minimizes waste and requires low energy to operate. Advances in microfluidics have been applied to many biomedical processes. For example, microfluidic chips have been developed for PCR amplification [27], microarrays [28], simulating organ-level function [29], and generation of emulsions [30]. Microfluidic devices are easily parallelized into arrays for high throughput and are modular, enabling sample preparation, processing, and analysis on one chip.

1.4.1 Microfluidic Generation of Microbubbles

Microfluidic devices for microbubble production are typically biphasic systems that direct gas and liquid (containing the shell material) phases through micrometer sized channels and apertures to shear microbubbles from a gas cone or jet. Several microfluidic device designs for microbubble production exist including: t-junction [31], co-flow [32], coaxial electrohydrodynamic atomisation (CEHDA) [33], and flow-focusing microfluidic devices (FFMDs) [34–39]. While all these designs are capable of producing monodisperse distributions of microbubbles, FFMDs, the focus of this study, have found preference as they are produced by casting polydimethylsiloxane (PDMS), a biocompatible synthetic polymer, onto

molds fabricated using conventional micro-photolithography [40], [41]. Photolithography allows intricate channel patterns to be produced at micrometer scales in a simple, low-cost, and time efficient fabrication process. FFMDs work by a capillary instability effect, where a gas is “focused” by liquid flow on both sides of the gas and forced through a small aperture or “nozzle” causing microbubbles to shear off the gas cone (Fig 1.3) . The microbubbles break off from the gas cone and travel into an expanding outlet. The expanding outlet geometry creates a velocity gradient that facilitates microbubble breakoff in a consistent location and manner.

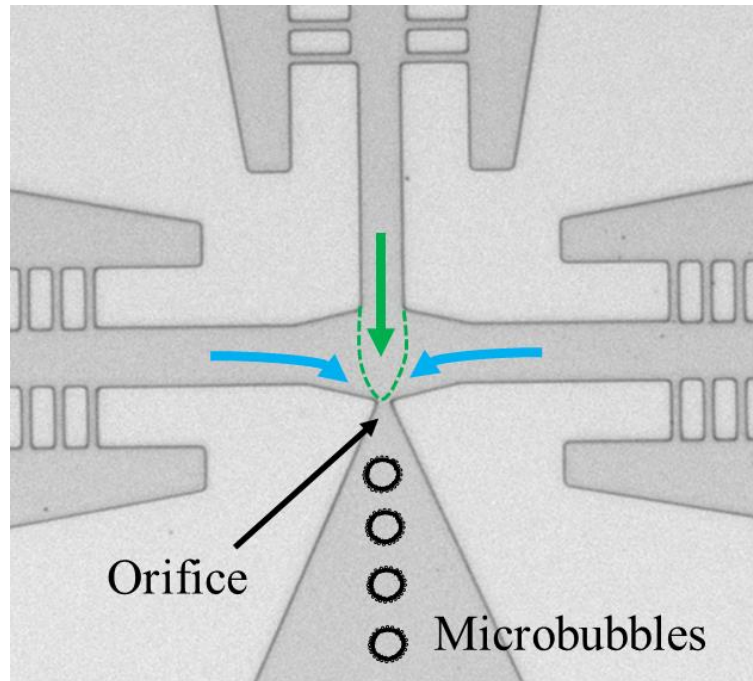


Figure 1.3: Schematic of a flow-focusing type microfluidic device. There is a central gas channel (green arrow) that is formed into a gas cone (green dotted line) by two liquid side flows (blue arrows). The gas cone is focused through a small orifice where shear forces cause microbubbles to break off in a uniform fashion. The microbubbles travel down an expanding outlet. The geometry of the outlet creates a velocity gradient where the highest velocity and shear force is focused at the orifice. This helps microbubbles break off at high speed in a sequential manner.

1.4.2 Microfluidic Interconnects

Microfluidic devices need to be interfaced to the outside world in order to introduce reagents and manipulate samples. This is typically done by using tubing interconnects. Interconnects range from simple “plug-and-play” type connections (Fig 1.4C) to sophisticated manifolds with an array of tubing supplying samples to many inlets. These connections are typically sealed by an adhesive, such as an epoxy or by luer lock type fitting (Fig 1.4A-B). A tight seal is necessary to prevent any leakage of material and loss of pressure at the interface of the connection [42]. In low-pressure settings, sometimes it is sufficient simply to plug the tube directly in the input without any sealant. One concern is that the interface of the interconnect has to be large enough so the connection is held in place and will not break off or detach. Additionally, a single microfluidic device may have multiple interconnects. These requirements typically limit the miniaturization and packaging of microfluidic devices [43].

Microfluidic chips are usually designed for bench top operation. Their already com-

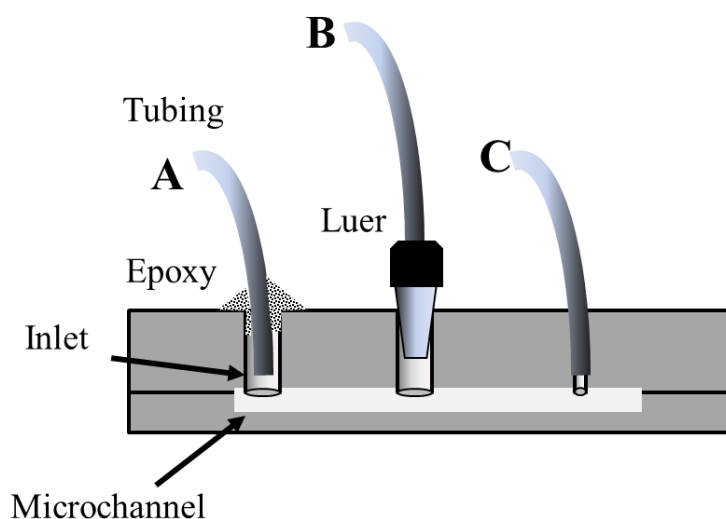


Figure 1.4: Schematic of different microfluidic interconnects. (A) Tubing interconnect formed by inserting the tube into an inlet then sealing the interface between the tube and the microfluidic device. Suitable for microfluidic chips made from elastomeric (e.g. PDMS) and hard (e.g. plastic, glass) substrates. Luer lock type connection where tubing is simply screwed in. Suitable for high pressurized systems and for microfluidic chips made from hard substrates. (C) Simple plug-and-play connection suitable for low pressure systems. Only works with elastic substrates that can expand and snugly fit when a tube with a diameter larger than the diameter of the inlet is inserted.

pact form factor means there has been little research to miniaturize these devices further for applications such as for *in vivo* operation within the body. Although work has been done on implantable microelectromechanical (MEMs) systems, their control is usually mediated electronically and thus do not require interconnects. Additionally they are typically limited to bio-sensing [44] or drug releasing applications [45]. Being able to operate microfluidic device *in vivo* via interconnects interfacing with users outside the body would allow for better manipulation of reagents and supply would not be limited to sample amounts that can fit within a microfluidic chip.

1.5 Specific Aims

Specific aim 1 (Chapter 2): To design a novel method for supplying the liquid (shell material) to a flow-focusing microfluidic device. We will develop a “flooded” method for supplying the liquid phase, where liquid interconnects will be replaced by a liquid-filled pressurized chamber or lumen. Reducing the number of interconnects allows FFMDs to be miniaturized to vascular dimensions, allowing FFMDs to generate and dispense microbubbles locally.

Specific aim 2 (Chapter 3): To develop a biocompatible albumin-coated microbubble with short half-life for real-time imaging and delivery. A proteinaceous microbubble will be characterized for half-life, acoustic properties, and therapeutics. These results will demonstrate the potential for a completely endogenous microbubble generated at the point-of-care from a patient’s own blood.

Chapter 2

Fabrication and Characterization of a Flooded Microfluidic Catheter Prototype for *In Situ* Microbubble Generation

2.1 Introduction

Flow-focusing microfluidic devices (FFMDs) are promising tools for generating monodisperse microbubbles. FFMDs for microbubble generation have been investigated extensively in the last decade. FFMDs were first used for liquid-liquid generation of droplets. Gañán-Calvo and Gordillo were first to demonstrate the production of gaseous microbubbles via a FFMD with a water-ethanol and water-glycerol formulation [32]. The method has since advanced to the production of lipid-coated microbubbles with size ranges appropriate for ultrasound contrast agents [37].

The most common shell material used with FFMDs is lipids due to their properties as discussed in chapter 1. A polyethylene glycol (PEG) emulsifier is usually incorporated on the shell to form an extended “brush” layer to prevent coalescence [46]. The brush layer provides steric hindrance so adjacent microbubbles do not get close enough to coalesce. Despite these efforts, at high FFMD production rates, lipid-coated microbubbles tend to coalesce. The high speed at which microbubbles are formed allows a finite amount of time for lipid to fully adsorb on the surface of the nascent microbubble. Thus, FFMDs are operated at low production rates, on the order of 10^3 - 10^5 microbubbles per second (MB/s).

For imaging studies, billions of microbubbles are usually administered. For example, Optison (GE Healthcare) contains approximately 5.0 - 8.0×10^8 MB/mL, and several milliliters

(>5 mL) can be injected per study [47]. These quantities are required to compensate for losses that occur during IV administration [48] and circulation as a result of filtration by the lungs and clearance by the liver or spleen [49–51]. At current production rates, using a single FFMD would require several hours to acquire enough microbubbles for a single dose, which is not feasible in a clinical setting.

Production rates can be increased by parallelizing several FFMD modules on a single chip [52–56]; however, these parallelized devices can be difficult to operate. Equal pressures need to be supplied to each gas and liquid inlet, which can require a complex 3D manifold [31] in order to maintain monodispersity across all FFMD modules. Although the polydispersity index of individual flow-focusing channels may be low, the pooled polydispersity index is often higher due to variations across microbubble generating channels [32].

In order to overcome these limitations, we propose the production of microbubbles *in situ* directly within the vasculature with a catheter rather than bench top production for storage. By producing microbubbles within the vasculature, loss due to injection and circulation is eliminated, thus significantly reducing the quantity of microbubbles necessary to provide sufficient contrast. FFMDs are ideal for intravascular production of microbubbles as they can produce microbubbles in a continuous process in real-time at a specified diameter and production rate. Unfortunately in their current design, FFMDs are difficult to miniaturize to vascular dimensions.

We have developed a new method for supplying the liquid phase to FFMDs that we believe will enable intravascular microbubble generation. As discussed in chapter 1, multiple interconnects restrict the size of FFMDs. In our design, we remove interconnects from the liquid inlets and supply the liquid phase via a pressurized chamber (Fig 2.1). The chamber is

filled with the liquid phase and pressurized (e.g. with a syringe). The pressure gradient drives the liquid phase into the microfluidic inlets that would otherwise have tubing interconnects.

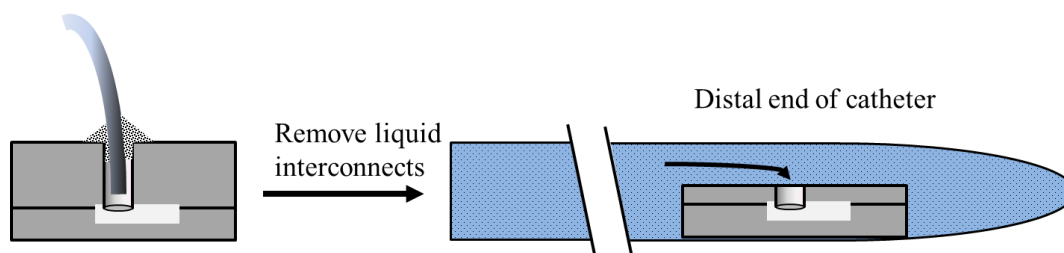


Figure 2.1: Method for supplying the liquid phase via a catheter. Liquid interconnects are removed and inlets directly coupled to a chamber, which is the lumen of the catheter. The lumen is filled with the liquid phase and pressurized to drive flow into the inlets (arrow). This allows the microfluidic device to be miniaturized because the device doesn't have to accommodate multiple interconnects. Microbubbles can be made *in situ* and dispensed at the distal end of the catheter.

This design demonstrates several advances over current designs. First, the number of tube-device interconnects are reduced as the inlet is open to the pressurized lumen of the catheter. Second, this design simplifies FFMD parallelization. Additional liquid inlets for supplying additional FFMDs can be introduced simply by drilling more inlets into the microfluidic device. This significantly reduces the footprint of the device, as a complicated 3D array of branching microchannels are not needed, and helps to ensure equal liquid pressure gradients across all nozzles [27], [33]. Finally, by simplifying production and reducing the footprint of FFMDs, the flooded design facilitates miniaturization and integration into catheters intended for applications in the peripheral (2-5 mm in diameter) or coronary (~1 mm in diameter) vasculature. This method of filling the lumen with the liquid phase is termed the “flooded” method.

In this chapter we demonstrate the fabrication and functionality of a flooded microfluidic device. We characterize the relationship between microbubble size, production rate, gas pressure, and liquid flow rate using a high speed camera. Our results show that the flooded

method allows FFMDs to be miniaturized to vascular dimensions without impacting microbubble production.

2.2 Materials and Methods

2.2.1 Microfluidic Device Fabrication

Flow-focusing microfluidic devices (FFMDs) were cast in polydimethylsiloxane (PDMS) (Sylgard 184, Dow Corning, Midland, MI) using a custom fabricated mold [40]. Molds were fabricated by spinning a negative photoresist (SU8-3025, Microchem, Newton, MA) onto a silicon wafer then exposing the wafer to UV through a 0.1 μ m spot size quartz mask (Microtronics Inc, Newtown PA) designed in AutoCAD (Autodesk, San Rafael, CA) (Fig. 2.2).

The FFMD was designed to have three inlets: two liquid inlets on either side of one central gas inlet (Fig 2.3). All microfluidic devices had the following features: 8 μ m wide nozzle, 8 μ m filters (Fig 2.3, black arrowhead) to prevent particulates from clogging the device, posts (Fig 2.3, red arrowhead) throughout the channels to prevent channel collapse, 35 μ m wide gas channel, 50 μ m wide liquid channels, and 20 μ m height. PDMS in a 10:1 base to curing agent ratio was poured onto the mold, degassed, and then cured at 80°C for 30 minutes. The device was then oxygen plasma treated and bonded to different substrates depending on the type of device. Two types of devices were fabricated, non-flooded and flooded FFMDs. Non-flooded devices were simply bonded to a clean piece of PDMS to form a closed microchannel network accessible via the inlets (Fig 2.2, 2.4).

Two versions of flooded FFMDs were produced: externally mounted flooded FFMDs (eFFMDs) and internally mounted flooded FFMDs (iFFMDs) (Fig 2.4). 10 mm square poly-

styrene cuvettes were used as surrogates to catheters. First, holes (0.65 mm) were in the cuvettes (Fisher Scientific Pittsburgh, PA) to create the liquid inlets and microbubble outlet ports (Fig 2.4 red arrowheads). eFFMDs were then mounted by plasma bonding (March II, Nordson March, Concord, CA) (60 W, 1 min) a PDMS device to the outside of a pre-drilled cuvette treated for 20 min with a 1% APTES solution [59]. Whereas iFFMDs were fabricated by first plasma bonding (25W, 30 s) a clean PDMS layer to a device before mounting the device to the interior of the cuvette with epoxy (Hysol RE2039 and HD3561, Henkel Corp. Mooresville, NC). Microbore PTFE tubing (Cole Parmer, Vernon Hills, IL) was then inserted into the gas inlet and sealed with epoxy. Finally, a PTFE tube for supplying the liquid phase was placed inside the cuvette prior to sealing the chamber with epoxy and hot melt glue. iFFMDs were also produced using a 3 mm square glass tube (S103, Vitrocom Mountain Lakes, NJ) and a 6 mm inner diameter glass pipette (Fisher Scientific Pittsburgh, PA).

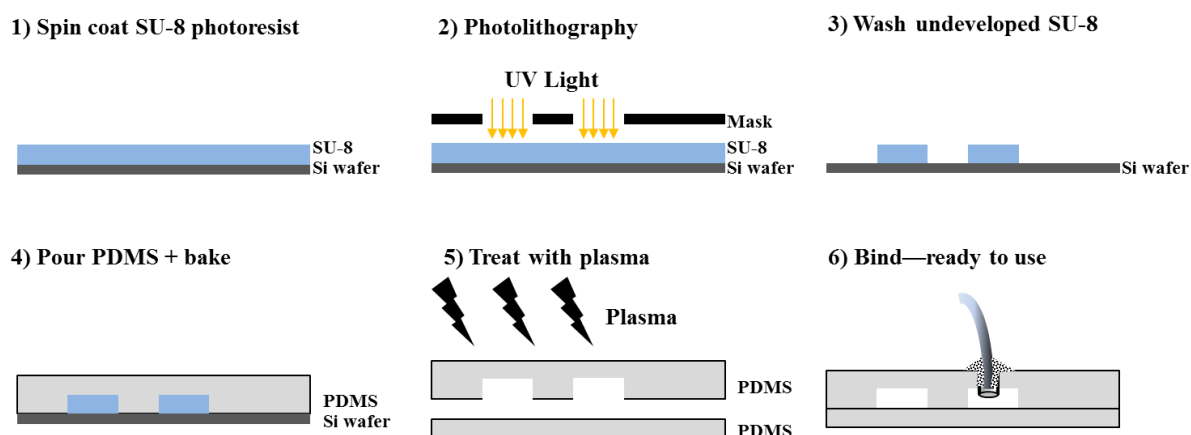


Figure 2.2: Schematic of steps for microfabrication of a non-flooded microfluidic device. SU-8 photoresist is spin coated onto a silicon (Si) wafer. A mask of the microfluidic network is placed on top and exposed to UV light. UV light causes photoresist to cross-link. The non-cross-linked SU-8 is washed away and the mold is finished. To make a microfluidic device, the PDMS is poured on the mold and baked. The PDMS with the channels and a plain piece of PDMS substrate are plasma treated and brought into contact to irreversibly bind. Interconnects are inserted and sealed to create the finished device.

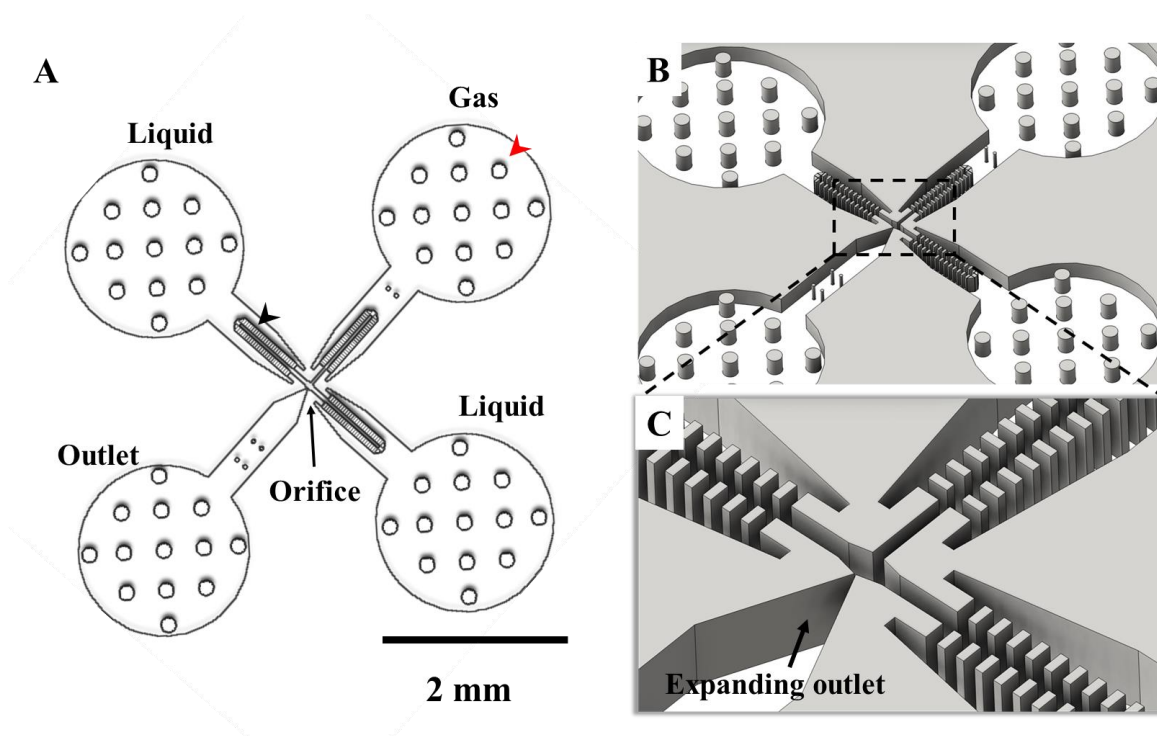


Figure 2.3: (A) Schematic of FFMD design. There are three inlets (two liquid, one gas), one microbubble outlet, posts (red arrowhead) to prevent microchannel collapse, filters (black arrowhead) to filter out particulates, and an orifice where microbubbles break off. (B) 3D rendering of the FFMD. (C) Zoom into the orifice showing the expanding geometry of the outlet.

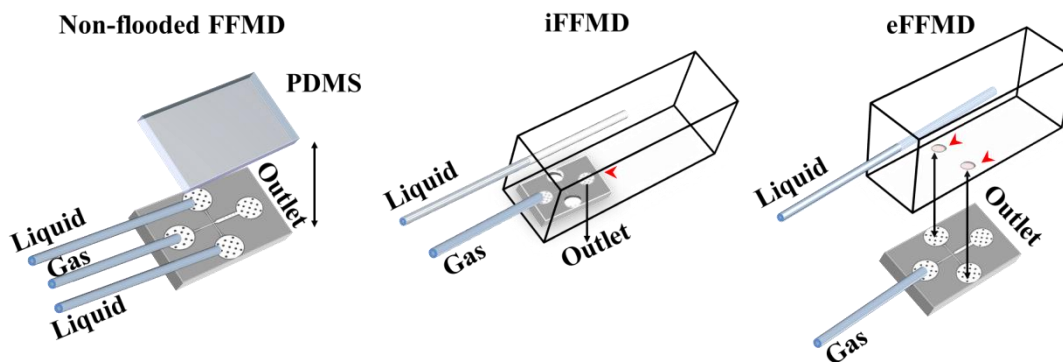


Figure 2.4: Schematics of non-flooded and flooded FFMDs. The liquid phase to non-flooded FFMDs were supplied by tubing interconnects. Flooded FFMDs were fabricated by first drilling access holes into the cuvettes (red arrowheads). For iFFMDs, the FFMD was mounted in the lumen of the cuvette. For eFFMDs, the FFMD was mounted to the outside of the cuvette. The liquid phase to flooded FFMDs was supplied by filling the lumen of the cuvette with the liquid phase and pressurizing with the chamber with a syringe pump.

2.2.2 Microbubble Formulation

Microbubbles were stabilized using polyethylene-glycol-40-stearate (PEG40S) (Sigma-Aldrich, St. Louis MO). PEG40S was dissolved at a concentration of 3 mg/ml in a solution of 10% glycerol, 10% propylene glycol, and 80% Millipore purified deionized water (GPW). The solution was sonicated (XL2020, Misonix, Farmingdale NY) with a ½ inch probe (40% power, 30 min) and filtered through a 0.45 µm syringe filter (Fisher Scientific Pittsburgh, PA). The gas phase consisted of highly purified nitrogen gas (GTS Welco Richmond, VA).

2.2.3 Microbubble Production

The liquid phase was supplied to the device using a syringe pump (PHD2000, Harvard Apparatus) at flow rates between 10-120 µL/min while the gas phase was applied at pressures between 34-69 kPa. Pressure was set using a two-stage regulator (VTS 450D Victor Equipment Company Thermodyne, St. Louis, MO) and digital manometer (06-664-21 Fisher Scientific Pittsburgh, PA).

Images of microbubble production within the microfluidic device were captured using an inverted microscope connected to a high speed framing camera (SIMD24, Specialised Imaging, Simi Valley, CA). Microbubble diameter and production rate were measured from the acquired images using ImageJ (v 1.46d NIH Bethesda, MD). The relationship between gas pressure, liquid flow rate, microbubble diameter, and production rate was investigated by incrementing the liquid flow rate in 2 µl/min step sizes at a constant gas pressure until microbubble production became unstable. Data was only collected for gas and liquid combinations that resulted in microbubbles less than 20 µm in diameter (i.e. less than the height of the

FFMD channels) to limit the effect of wall interaction on microbubble production dynamics. The polydispersity index (PDI) was calculated (equation 3) for each flow rate and monodispersity was considered to be PDI less than 10%.

2.3 Results and Discussion

2.3.1 FFMD Fabrication

Both externally mounted flooded FFMDs (eFFMDs) and internally mounted flooded FFMDs (iFFMDs) were successfully fabricated. The reduction in number of interconnects allowed FFMDs to be reduced in size. The smallest iFFMD manufactured to date measures 14.5 x 2.8 x 2.3 mm, where the longitudinal dimension is not restricted in a vessel. While eFFMDs and iFFMDs share the same fundamental design, a major difference is the pressure applied to the microfluidic device. In eFFMDs, the channels in the microfluidic device are not subject to the pressures inside the liquid chamber; while in the iFFMD, the microfluidic device needs to withstand the pressure necessary to drive liquid into the microfluidic inlets.

2.3.2 Microbubble Production and Characterization

Microbubble production could be divided into five distinct regimes [60], [61] (Fig 2.5). The flow rate that defined the transition points of these regimes depended on gas pressure. Overall, increases in the gas pressure increased the minimum flow rate at which a regime began. Microbubble production was most stable when the produced microbubbles had diameters less than the height of the channel but greater than the nozzle width, which we term the stable regime. In addition, maximum production rate always occurred within the stable regime. As a result, flooded FFMDs were only operated and characterized in this regime.

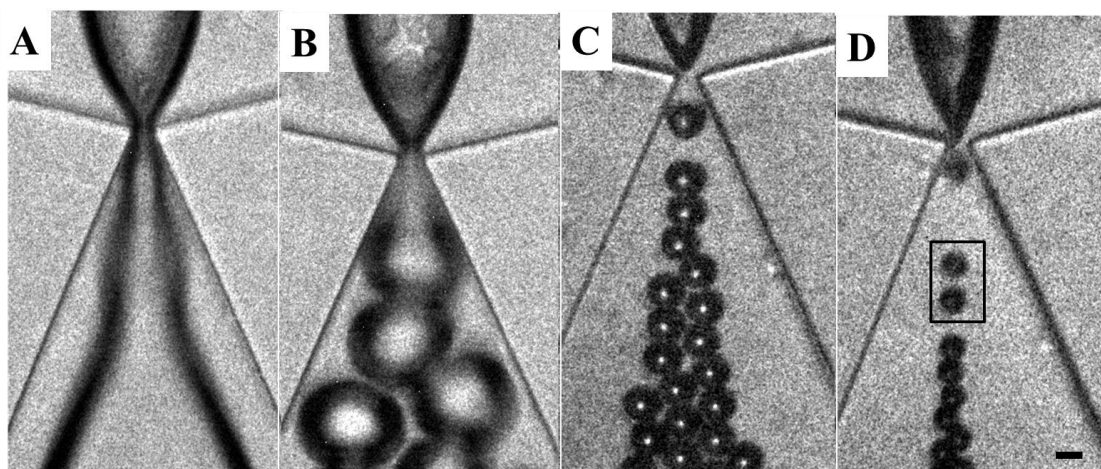


Figure 2.5: Microbubble production regimes of flooded FFMDs. Scale bar = 10 μm for all figures. (A) Regime I: Overpressure ($< 34 \mu\text{L/min}$)—the gas pressure overwhelms the liquid flow rate and no microbubbles are produced. (B) Regime II: Cylindrical ($34\text{--}60 \mu\text{L/min}$)—microbubbles are larger than the height of the microfluidic channel resulting in the production of non-spherical microbubbles. (C) Regime III: Stable ($60\text{--}80 \mu\text{L/min}$)—microbubbles with diameters less than the height of the channel but greater than the nozzle width are stably produced. (D) Regime IV: Unstable ($80\text{--}92 \mu\text{L/min}$)—microbubble production becomes unstable and can result in doublet formation (i.e. two microbubbles in quick succession followed by a delay in microbubble production – black box) and microbubbles with diameters less than the nozzle width. Regime V: Under-pressure ($> 92 \mu\text{L/min}$)—liquid flow overwhelms the gas pressure and no microbubbles are produced (not shown). Flow rates are representative for a gas pressure of 55.2 kPa.

While it was possible to produce microbubbles with diameters that were smaller than the width of the nozzle, microbubble production would often become unstable, due to high liquid flow rates inhibiting the gas cone from entering the orifice and pinching off microbubbles. Production rate dropped precipitously and satellite microbubbles (i.e. microbubbles that form in quick succession followed by a pause in production) formed (Fig 2.5D).

While eFFMDs were capable of stably producing microbubbles at high production rates, iFFMDs were only able to produce microbubbles for approximately 10 minutes at a time during which microbubble diameter would decrease until production ceased. This observation was likely due the microchannels collapsing as the chamber is pressurized, as PDMS is a compliant material. As a result gas flow rate would decrease, resulting in smaller microbubbles, until flow ceases altogether. The eFFMD design mitigates the problem by placing the

FFMD outside the pressurized liquid chamber and thus preventing the collapse of the gas channel.

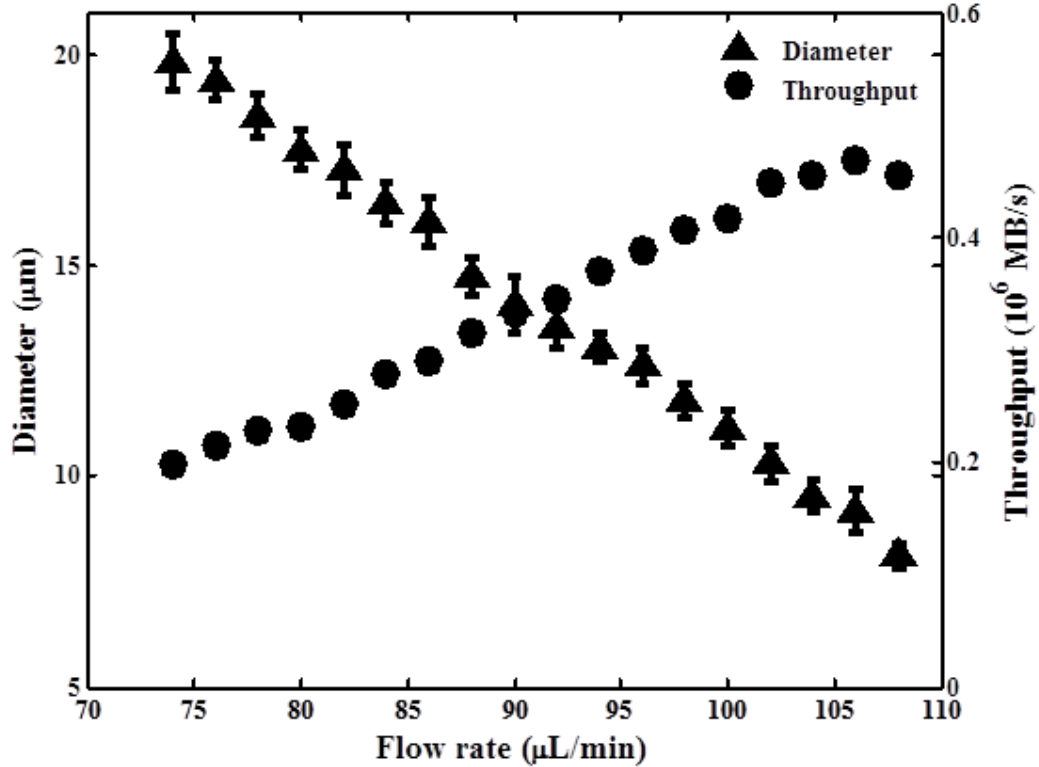


Figure 2.6: Production curves for an eFFMD operating at 68.9 kPa. Production rate increased approximately linearly with flow rate. Concurrently, microbubble diameter decreased linearly with flow rate. This property may be desirable as smaller microbubbles can be generated at high production rates, compensating for any reduction in bioeffects due to a decrease in microbubble size, such as for drug delivery. eFFMDs exhibited similar production characteristics to non-flooded FFMDs, showing that the flooded method does not hinder performance and is a good substitute for traditional interconnects.

eFFMDs were characterized at a gas pressure of 68.9 kPa. At this constant gas pressure, microbubble diameter decreased linearly with increasing liquid flow rate ($R^2 > 0.98$) (Fig 2.6). The smallest stable microbubble was produced prior to transition out of the stable regime. The smallest microbubble produced approached the width of the orifice. Production rate at constant pressure increased linearly (Fig 2.4) with increasing liquid flow rate ($R^2 > 0.95$), with the maximum production rate occurring prior to transition out of the stable regime. The maximum production rate for a given pressure also increased with increasing pressure.

Overall, the diameter of the smallest microbubble produced was 8.1 μm and the maximum production rate observed was 470,000 MB/s (Table 2.1). These trends are observed in non-flooded FFMDs as well, suggesting that the fluid dynamics are similar in eFFMDs. This demonstrates that the flooded method does not hinder FFMD performance and that it is a feasible substitute for traditional interconnects, allowing FFMDs to be miniaturized. The flooded method allows parallelization without increasing the number of interconnects. Thus production rate may be increased several fold by operating several devices in parallel.

At 68.9 kPa, the average PDI was calculated to be 3.5%, which is consistent with those observed for previous FFMDs (Fig 2.7). This value is well below our monodispersity criterion ($\text{PDI} < 10\%$). We demonstrate the production of stable monodisperse microbubbles at high production rates using a simple emulsifier (PEG40S) stabilized with glycerol and propylene glycol. These microbubbles do not exhibit a half-life as long as that observed for lipid microbubbles. By generating and dispensing microbubbles *in situ*, however, long half-lives are no longer a strict requisite as microbubbles no longer need to circulate systemically.

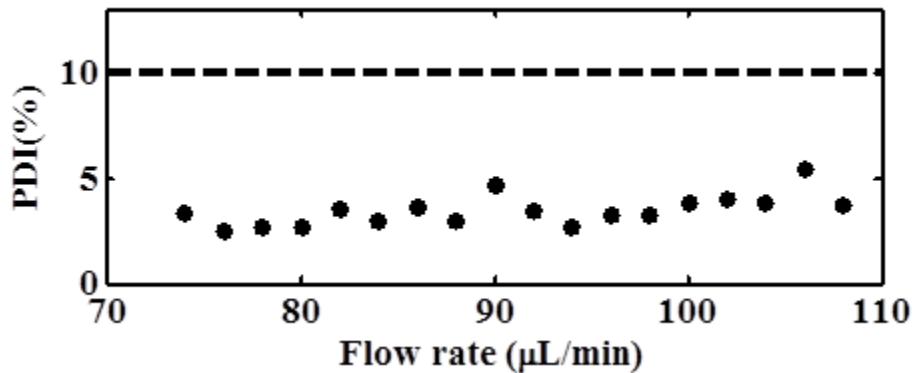


Figure 2.7: Microbubble polydispersity index (PDI) at the orifice of a eFFMD at a pressure of 68.9 kPa. The average PDI was 3.5%, which is an excellent improvement over conventional sonication methods.

	iFFMD	eFFMD
Smallest Diameter (μm)	9.8 \pm 0.5	8.1 \pm 0.3
Production Rate @ Smallest Diameter (MB/s)	3,600	450,000
Flow rate ($\mu\text{L}/\text{min}$)	10	108
Gas Pressure (kPa)	34.5	68.9
Max Production Rate (MB/s)	4,600	470,000
Diameter @ Max Production (μm)	16.5 \pm 0.8	9.2 \pm 0.5
Flow rate ($\mu\text{L}/\text{min}$)	10	106
Gas Pressure (kPa)	41.4	68.9

Table 2.1: Microbubble production for a single nozzle iFFMD and eFFMD. Liquid phase was 3 mg/mL PEG40S in GPW. Gas phase was nitrogen.

2.4 Conclusions

Although promising results were reported, more progress is needed to further reduce FFMD dimensions for intravascular applications. This can be done by improving the performance of iFFMDs, which suffered from microchannel collapse due to pressurization of the liquid chamber. A more rigid substrate such as Poly(methyl methacrylate) (PMMA), glass, or plastic would likely improve microbubble production; however, a different fabrication technique would be necessary, such as wet etching or hot embossing. Furthermore, dimensions can be reduced by a new microfluidic design. Our current inlets were designed for conventional interconnects. Using the flooded method, however, smaller inlets can be used, as they are now accessed by pressurization via drilled holes without any necessary tubing or epoxy. Also microfluidic designs that utilize the longitudinal dimension of the catheter lumen, rather than the width dimension, can be investigated as a strategy for reducing microfluidic footprint.

In this chapter, we report on a novel method of supplying the liquid phase to a FFMD via a pressurized flooded chamber. By coupling the FFMD to a flooded chamber, we reduce the number of interconnects and simplify FFMD miniaturization. We created several prototype surrogate catheters and demonstrated the production of microbubbles at production rates up to 470,000 MB/s with dimensions appropriate for intravascular applications. This method would allow the user to supply the liquid and gas phases through a catheter via ports outside the body. Additionally, by generating microbubbles locally, novel microbubble compositions may be explored, such as those with short half-lives that dissolve quickly, potentially reducing emboli risk. Furthermore larger microbubbles may be used for increased acoustic signal and bioeffects. These designs are the subject of the following chapter.

Chapter 3

Synthesis and Characterization of Transiently Stable Albumin-Coated Microbubbles

3.1 Introduction

Producing microbubbles near the site of interest enables investigation of novel microbubble compositions that are not feasible in current implementation of FFMDs. In chapter 2, we produced transiently stable microbubbles from a simple polyethylene-glycol-40-stearate (PEG40S) emulsifier shell and nitrogen. However, PEG40S is not naturally found in the body and high concentrations can lyse cell membranes. Lipid formulations require complex preparation to disperse the lipid in an aqueous phase and production rates of flow-focusing microfluidic devices are low due to high lipid viscosity and coalescence. Additionally, polymer formulations may be highly viscous and thus suffer from low production rates [62]. Since microbubble stability is no longer a concern, we investigated using semi-stable shell materials.

Albumin as a stabilizing shell material for microbubbles has been extensively investigated [6], [13]. Albunex, the first FDA approved microbubble, was composed of denatured human albumin and an air core [63]. Optison superseded Albunex, replacing the air core with octafluoropropane—a highly insoluble gas—thus increasing microbubble stability and contrast duration to several minutes [44]. Microbubbles stabilized using an albumin shell—whether developed commercially or in-house—have been shown to enhance imaging applications, such as molecular targeting [64], [65], and therapeutic applications, such as gene transfection [66–68] or sonothrombolysis [7], [69]. Although alternative shell materials (e.g. lipid,

polymer, surfactant) exist, albumin continues to be a relevant material because of its ability to form stable microbubbles, its biocompatibility, and its excellent safety profile [63], [70], [71].

Microbubbles are currently designed to be stable enough to survive systemic circulation and provide an adequate duration of contrast enhancement. As a result, however, microbubbles must be less than 10 μm in diameter in order to avoid entrapment in the microcirculation [49]. Larger microbubbles have been shown to provide increased acoustic contrast [72], [73] and increased sonoporation [11], [55]. By producing microbubbles with a microfluidic device near the diseased site, larger transiently stable microbubbles with greater bioeffects and reduced risk for gas emboli can be realized.

Several factors have inhibited the adoption of albumin for forming proteinaceous microbubbles with a bench top FFMD. Conventional preparations utilize heating and sonication at high temperatures to denature albumin and form disulfide bonds to produce a rigid cross-linked shell [10]. Generation rates can be high in microfluidic devices so there is a finite amount of time ($\sim 10^{-3}$ - 10^{-6} s) for microbubble formation. Albumin must rapidly adsorb and spread onto the gas/liquid interface to fully encapsulate the gas and an incomplete coating can lead to microbubble coalescence. In addition, it may be difficult to denature and cross-link albumin without long serpentine channels and heating elements in a FFMD, features that may limit miniaturization of FFMDs. However, since long-term stability is not a requisite for our intended applications, cross-linking is not necessary. Non-cross-linked albumin has a high surface tension (i.e. Laplace pressure) [74], resulting in short lived emulsions [10], [75], which poses a problem in conventional applications but is not a concern with localized production and delivery.

Optimizing albumin microbubble production in a FFMD is also a step towards utilizing whole blood plasma as a medium for fabricating microbubbles. While plasma microbubbles could be generated by sonication, a microfluidic method would facilitate a completely lab-on-a-chip method for separating blood plasma from whole blood [76], and generating and dispensing microbubbles from one device. A patient's own blood could potentially be used at the point-of-care to generate a perfectly biocompatible contrast agent.

In this chapter, we demonstrate production of nitrogen filled albumin-coated microbubbles from a FFMD using both fractionated bovine serum albumin and fresh bovine plasma. The FFMD was characterized for microbubble diameter, production, and coalescence using a high-speed camera. Microbubble stability was characterized optically and acoustically. Large diameter microbubble enhanced drug delivery was investigated using a custom flow chamber with a cell monolayer under physiological flow conditions. Ultrasound contrast improvements were determined using a clinical ultrasound scanner and a flow phantom.

3.2 Materials and Methods

3.2.1 FFMD Fabrication

Non-flooded flow-focusing microfluidic devices were fabricated as described in chapter 1 with a few modifications. After plasma bonding, microfluidic devices were heated at 70°C for 1 hour prior to use to ensure hydrophobicity of the channels to allow for a stable gas cone. The final dimensions of the gas and liquid channels were 35 and 50 μm wide, respectively, the nozzle was 7 μm wide and all channels were 27 μm tall.

3.2.2 Microbubble Fabrication

The liquid phase consisted of 3 or 5% (w/v) bovine serum albumin (BSA) dissolved in a solution of isotonic saline (0.9% NaCl) or a solution of 2.5% glycerol, 2.5% propylene glycol, and 95% (v/v) isotonic saline (2.5% GPS). Dextrose was added at a concentration of 10% (w/v) to either solution as needed. All chemicals were purchased from Sigma-Aldrich (St. Louis, MO). A pharmaceutical grade preparation of 5% human serum albumin (HSA) (BSL Behring, King of Prussia, PA) was also tested. Albumin concentration was measured with a spectrophotometer (NanoDrop 1000, Thermo Scientific, Wilmington, DE) at 280 nm wavelength and a molar extinction coefficient of 6.7 L/mol-cm. Viscosity (η) was measured with an Ubbelohde viscometer (Cannon Instrument Company, State College, PA) at 23°C. The gas phase consisted of 99.998% nitrogen (GTS Welco, Richmond, VA). The FFMD liquid flow rate was set via syringe pump (PHD Ultra, Harvard Apparatus, Holliston, MA), while the gas pressure was set via a two stage pressure regulator.

3.2.3 Microbubble Characterization

To characterize the microbubbles generated from a FFMD, images were taken at the microfluidic orifice using a high speed camera attached to an inverted microscope. Images were taken downstream (~1.7 mm) to observe microbubble coalescence. Any microbubble resulting from the fusion of two or more microbubbles was considered a coalesced microbubble. Microbubble production rate and size was measured using ImageJ. Monodispersity was defined as polydispersity index (PDI) less than 10%.

Microbubble stability was estimated optically and acoustically. In the optical method, microbubbles were collected at room temperature (23°C) under a glass slide at the output of

the FFMD and videos were taken with a digital camera (Canon T3i, 29.97 fps, Canon, Lake Success, NY) to observe microbubble dissolution. Every 100th frame was analyzed and the number of microbubbles between 4-38 μm in diameter was counted using a custom circular Hough transform algorithm [77] developed in Matlab (Mathworks, Natick, MA) (see appendix A). The lower limit was selected based on the optical resolution of the images. The upper limit was selected to be double the largest microbubble expected to be produced. The microbubble half-life was defined as the time until half the maximum number of microbubbles (T_{mb}) remained in the field of view. In the acoustic method, a temperature controlled (16, 23, 37°C) 200 mL solution of microbubbles in air-saturated DI water was imaged with a clinical scanner—Siemens Sequoia 512 with 15L8 linear array. A contrast agent specific nonlinear mode (contrast pulse sequences [CPS]) at a center frequency of 7 MHz and mechanical index (MI) of 0.2 was used to minimize ultrasound destruction of microbubbles. Microbubbles were produced with the FFMD until the ultrasound image was saturated with microbubbles after which the FFMD was removed. The image intensity over time was analyzed in Matlab by averaging a 30x30 pixel window in each frame. Each time-intensity curve was aligned by peak intensity and averaged ($n \geq 5$). Microbubble half-life was calculated as the time until half the maximum intensity (T_i) was observed.

3.2.4 Cell Culture and Calcein Delivery

Primary rat aortic smooth muscle cells (SMCs) were plated on Thermanox coverslips (Nunc, Rochester, NY) at a density of 5×10^3 cells/cm² and incubated at 37°C in a 5% CO₂ environment. The SMCs were cultured in growth media (DMEM/F12 plus 10% fetal bovine

serum, Gibco, Grand Island, NY) and were allowed to reach 100% confluency prior to experimentation.

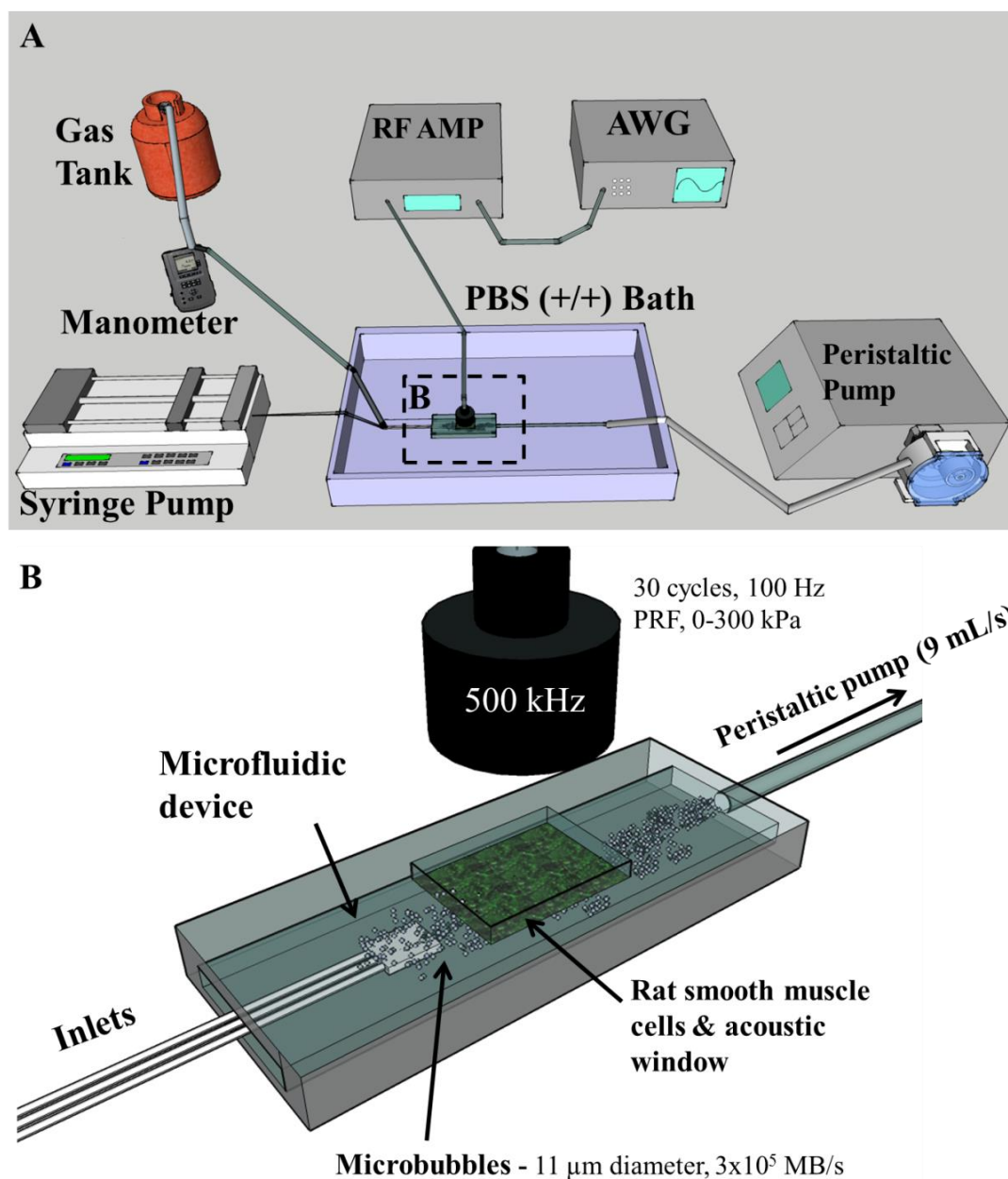


Figure 3.1: Schematic of model drug delivery with a FFMD. (A) Flow through the flow chamber was provided by a peristaltic pump. Two syringe pumps were used, one for supplying the liquid phase to the FFMD and another for supplying the calcein (not shown). Gas was supplied with a gas tank monitored by a manometer. The waveform was supplied by the AWG and amplified by the RF AMP. (B) Enlarged schematic of the flow chamber. The microfluidic device is placed upstream and calcein and microbubbles are delivered to SMCs. An acoustic window was created so ultrasound can penetrate the flow chamber without significant reflections.

A custom flow chamber (Fig 3.1B) designed for laminar arterial flow was constructed from acrylic with dimensions 0.2 cm x 2.4 cm x 18 cm and an acoustic window (50 μ m thick Mylar, McMaster-Carr, Atlanta, GA) half-way down its length. A Thermanox coverslip with SMCs was placed within the flow chamber and was submerged in 155 mM phosphate buffered saline with calcium and magnesium (PBS +/+) (Gibco) at 37°C. A peristaltic pump (Unispense 340, Wheaton Industries, Millville, NJ) was used to pull PBS ++ through the chamber at an average flow rate of 9 mL/s. A FFMD, generating 11 μ m diameter monodisperse microbubbles at a rate of 660,000 MB/s, was placed inside the custom flow chamber. Calcein was supplied using a separate syringe pump for a final concentration of 0.05 mg/mL within the flow chamber.

Ultrasound was applied by a 1 inch diameter 500 kHz single-element ultrasound transducer (V301 Olympus Panametrics, Waltham, MA) at half the focal distance above the acoustic window. Delivery was performed with a 30 cycle, 500 kHz sinusoid at a pulse repetition frequency (PRF) of 100 Hz. The waveform was supplied by an arbitrary waveform generator (AWG3022B, Tektronix, Beaverton, OR) and amplified by a 60 dB RF power amplifier (A-500 ENI, Rochester, NY) (Fig 3.1A). An ultrasound center frequency of 500 kHz was selected to best match the resonant frequency of the microbubbles [78]. Only the effect of ultrasound peak negative pressure (PNP) on drug delivery was investigated. PNP of 0, 100, 200, 300 kPa were investigated. Sonoporation was induced using ultrasound for two minutes while microbubbles and calcein flowed through the flow chamber. Following sonoporation, cells were allowed to reseal for 2 minutes in plain PBS ++ without flow, microbubbles, or calcein. Cells were then stained for cell death with propidium iodide (PI) at a concentration of 25

$\mu\text{g/mL}$ for 30 minutes at 37°C . Cells were imaged using fluorescence microscopy within 6 hours after PI staining.

3.2.5 Plasma Microbubbles

Bovine blood from an FDA approved abattoir was collected in 1.86 mg/mL EDTA. The plasma was separated from the blood by centrifugation at 500 g for 30 min at 20°C to obtain a clear orange/pink supernatant. Glycerol and propylene glycol were added to the plasma at a volume concentration of 2.5% each (2.5% GP). Large aggregates and remaining red blood cells were filtered out using 8 and $2.5\text{ }\mu\text{m}$ pore-size filter paper (Grade 2, 5, Whatman, Maidstone, ME) followed by $0.45\text{ }\mu\text{m}$ pore syringe filters (Fisher Scientific, Waltham, MA). The plasma solution was used within 7 days of collection and was supplied to the FFMD as described above.

Plasma microbubbles were imaged in a gelatin flow phantom— 6% (w/v) gelatin (Type B, Fisher Scientific) and 1% (w/v) Agar (Fisher Scientific)—with a 4 mm diameter lumen to simulate contrast enhancement in a blood vessel (Fig 3.6A). A FFMD producing $16\text{ }\mu\text{m}$ diameter plasma stabilized microbubbles at a rate of $125,000\text{ MB/s}$ was placed in 100 mL bovine blood under constant agitation. The blood and microbubbles were pulled through the flow phantom at a flow rate of 105 mL/min using a syringe pump. Microbubbles were imaged with the Sequoia 512 (CPS mode, center frequency = 7 MHz , $\text{MI} = 0.2$). Microbubble stability in the flow phantom was observed by stopping microfluidic production and flow and measuring the T_i . Ultrasonic destruction of microbubbles was investigated by stopping flow, increasing the MI to 1.9 , and measuring T_i .

3.2.6 Statistical Analysis

In all cases, Student t-tests were used to determine statistical significance between experimental conditions. A p-value less than 0.05 was considered to be significant. For BSA microbubble stability studies, at least five trials were conducted for the acoustic and optical determinations. For the bovine plasma microbubbles in blood, stability and destruction was analyzed by conducting four trials each at 0.2 MI and 1.9 MI.

For the cell delivery, each pressure condition was investigated in triplicate. The number of cells that internalized calcein and the number of nuclei stained with PI in each image were counted. Percentages were calculated using the total number of cells prior to insonation, as ultrasound can cause cells to dislodge *in vitro* (Liu et al. 2012). Cell dislodgement was calculated as the difference between the cells remaining on the insonated coverslip and the number of cells on the control coverslip.

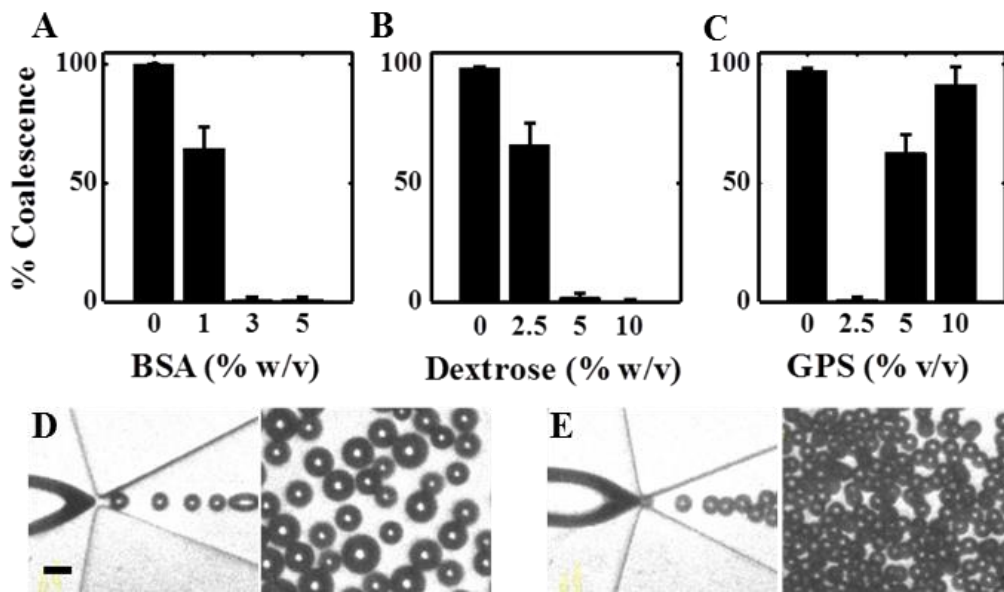


Figure 3.2: Effect of different components on microbubble coalescence. Microbubbles were imaged downstream of a FFMD operating at a pressure of 58.6 kPa. At a constant concentration of 10% dextrose, (A) increasing BSA prevented coalescence. At a constant concentration of 3% BSA, (B) increasing dextrose prevented coalescence. (C) An optimal concentration of 2.5% GPS was required to prevent coalescence. (Plotted as mean + one standard deviation, $n = 3$). Representative high-speed images of coalesced microbubbles (D) and stable monodisperse microbubbles (E) at the nozzle and further downstream of the FFMD are shown (scale bar = 20 μm).

3.3 Results and Discussion

3.3.1 BSA Microbubble Coalescence

Microbubbles with diameters between 10-20 μm were successfully produced at rates ranging $1-6 \times 10^5$ MB/s at gas pressures and liquid flow rates of 48.3-68.9 kPa and 50-80 $\mu\text{L}/\text{min}$, respectively. At these high production rates, however, the microbubbles generated from BSA alone tended to coalesce. Microbubbles pinched off at uniform diameter at the nozzle but coalesced downstream to form larger microbubbles with a polydisperse size distribution (Fig 3.2D). At a constant concentration of 10% dextrose, increasing BSA concentration prevented coalescence (Fig 3.2A, E). At a constant concentration of 3% BSA, higher concentrations of dextrose (5-10%) eliminated microbubble coalescence downstream, while an optimum concentration of 2.5% GPS eliminated coalescence (Fig 3.2B-C). Similarly for 5% HSA, higher concentrations of dextrose (5-10%) eliminated microbubble coalescence—all further experiments were conducted with BSA as a surrogate. A solution of only 10% dextrose in saline or 2.5% GPS or both failed to produce stable microbubbles.

A solution of 3% BSA had a viscosity of 1.10 cP. Adding 2.5% GPS increased the viscosity to 1.28 cP. Bulk liquid viscosity has been found to prevent microbubble coalescence by increasing the coalescence time [79] and also facilitate coalescence by increasing the interaction between microbubbles [80]. Thus, these two opposing effects may explain the optimum GPS concentration (2.5%) that was necessary to form stable albumin-coated microbubbles. Glycerol and propylene-glycol has also been shown to prevent coalescence for lipid-coated microbubbles [81]. 10% dextrose also increased the viscosity ($\eta = 1.42$ cP). Dextrose has been shown to stabilize sonicated albumin microbubbles, resulting in longer contrast duration [82] or increased therapeutic delivery [66]. The mechanism behind these observations has not

been entirely elucidated. Browning et al. [66] has suggested that dextrose may be glycosylating albumin leading to a more stable shell. However, no evidence was detected from mass spectroscopy of samples of 3% BSA and 10% dextrose (data not shown). Since there was no heating step in our microfluidic system, it was unlikely that there was any significant glycation. Instead, dextrose may have the same viscosity effect as GPS—alternatively, dextrose may stabilize the shell by initially adsorbing on the surface of nascent microbubbles. Although more studies are needed to elucidate the exact mechanism, both these mechanisms would allow more time for albumin to completely coat the microbubble and prevent coalescence. No significant difference between formulations was found in microbubble stability optically and acoustically, suggesting similar microbubble coatings for the two formulations.

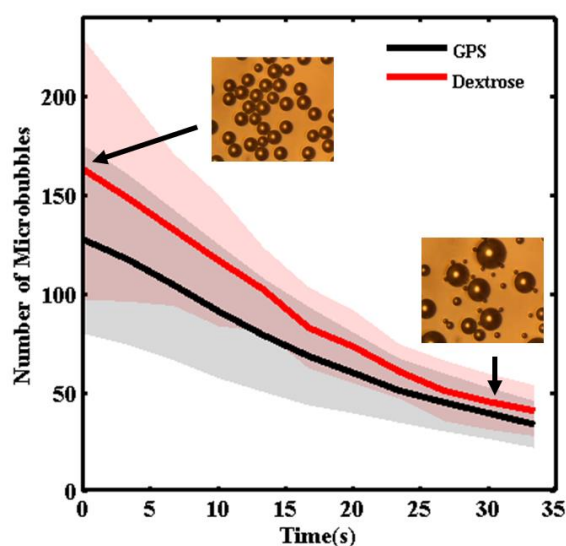


Figure 3.3: Optical determination of microbubble half-life. Microbubbles were collected with a glass slide and videos taken at 23°C to evaluate microbubble half-life for a solution of 3% BSA with 10% dextrose ($T_{mb} = 27.0 \pm 5.3$ s) or 2.5% GPS ($T_{mb} = 26.9 \pm 5.4$ s). There was no statistical significance in the measured T_{mb} (time until half maximum number of microbubbles) between the two formulations. The microbubbles were produced at 12 μ m in diameter. (Plotted as mean [solid] \pm standard deviation [shaded], $n = 6$).

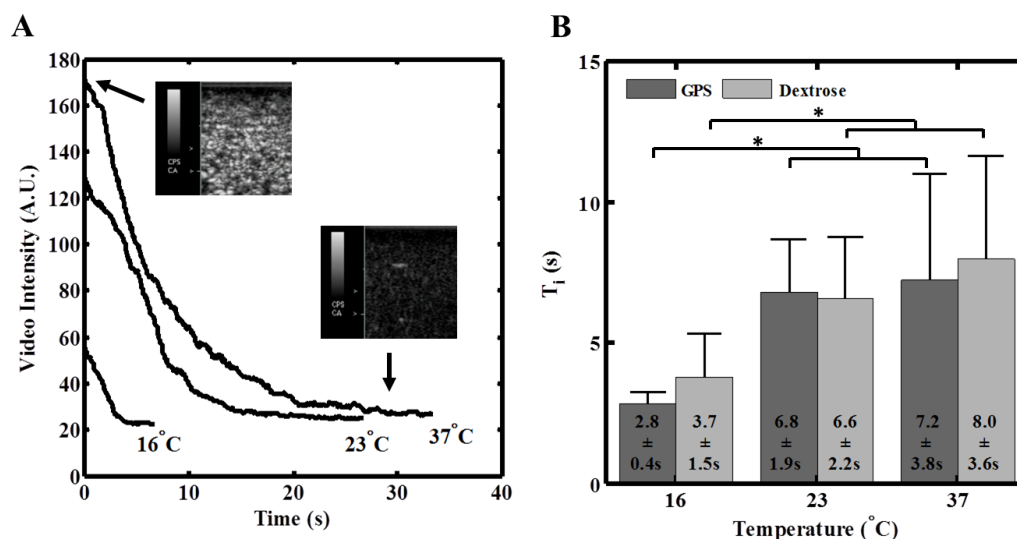


Figure 3.4: Acoustic determination of microbubble half-life. (A) For a 3% BSA and 2.5% GPS formulation, decrease in contrast was dependent on temperature. A 3% BSA and 10% dextrose formulation showed similar results (not shown). Dynamic range scale = 100 dB, and gain = 0 dB in ultrasound images. (B) The T_i (time until half maximum image intensity) for the two formulations at three temperatures. The microbubbles were 13-14 μm in diameter. (Plotted as mean + standard deviation, $n \geq 5$, * = $p < 0.05$).

3.3.2 BSA Microbubble Stability

Using optical microscopy, microbubbles started out monodisperse but quickly went through Ostwald ripening [8], with shrinking microbubbles collapsing completely due to Laplace pressure and growing microbubbles persisting for the duration of observation (~2 mins) (Fig 3.3 images). The T_{mb} of microbubbles fabricated from 3% BSA with either 10% dextrose or 2.5% GPS at 23°C were 27.0 ± 5.3 s and 26.9 ± 5.4 s, respectively (Fig 3.3). There was no statistically significant difference between the two formulations.

Using the Sequoia 512 scanner, the T_i at 23°C was measured to be 6.3 ± 2.3 s and 6.8 ± 1.9 s for a solution of 3% BSA with either 10% dextrose or 2.5% GPS, respectively. The T_i determined at 16°C was statistically different ($p < 0.05$) from 23°C and 37°C for the respective formulations (Fig 3.4), likely contributed to shrinking of microbubbles dictated by the ideal gas law. There was no statistically significant difference between the two formulations for the respective temperatures.

Microbubble lifetimes were evaluated in air-saturated media to more closely approximate the environment of blood found *in vivo*. Nitrogen filled microbubbles maintained their monodispersity after exiting the FFMD and quickly dissolved (Fig 3.3 images). Under optical observation, the microbubbles were static and thus exhibited longer stability than microbubbles observed acoustically (i.e. $T_{mb} > T_i$) under constant mixing. Since microbubbles would be subject to constant agitation *in vivo*, the latter method is likely a better indication of microbubble stability *in vivo*.

Since neither heat nor sonication was used, there was unlikely to be significant cross-linking between albumin molecules meaning that albumin was likely in a non-cross-linked or native conformation. Thus, weaker non-covalent forces (hydrogen bonds and hydrophobic interactions) may primarily be responsible for the formation of the shell [83], resulting in the rapid dissolution of the microbubbles. While unstable microbubbles would not be useful for systemic administration, they are advantageous in that larger microbubbles can be employed for greater therapeutic effect without persisting for long durations. The microfluidic platform potentially allows the user to tailor microbubble lifetime by controlling microscale heating, a technique which has been demonstrated in microfluidic/bioreactor technology [84], to induce protein denaturation and cross-linking. Another option is to replace the soluble gas core with a lower solubility gas (e.g. perfluorocarbon) to extend microbubble lifetime, as demonstrated in chapter 3.

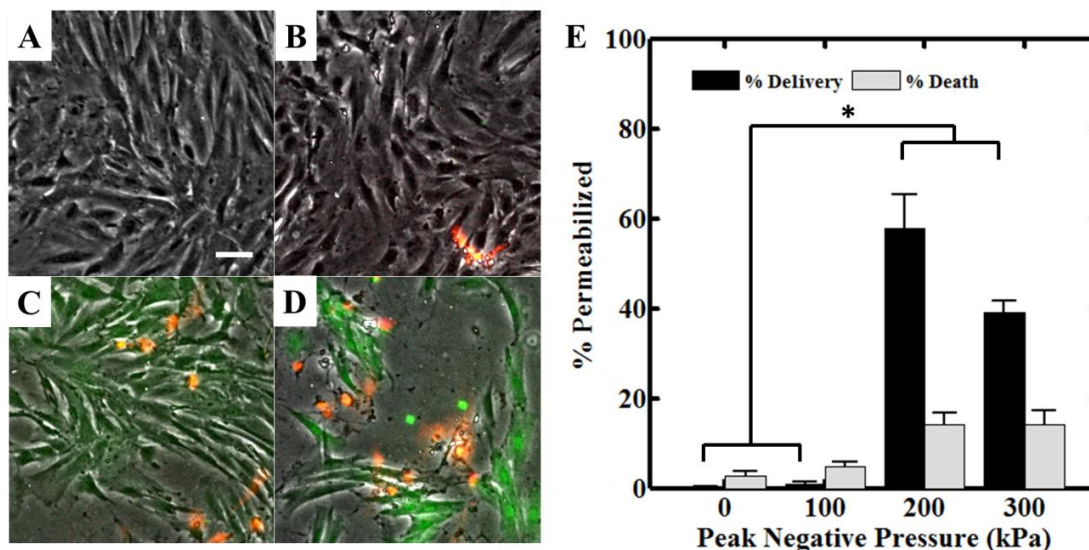


Figure 3.5: (A-D) Representative fluorescence microscopy images of rat aortic smooth muscle cells following calcein delivery for peak negative pressures of 0, 100, 200, 300 kPa, respectively. Green fluorescence indicates calcein internalization while orange indicates cell death (scale bar = 50 μ m). Flow rate was maintained at 9 mL/s—microbubbles were composed of 3% BSA, 2.5% GPS, and nitrogen produced with 11 μ m diameter at 660,000 MB/s. (E) Measured calcein delivery efficiency and percent cell death at different ultrasound peak negative pressures. (Plotted as mean + standard deviation, $n \geq 3$, * = $p < 0.0001$).

3.3.3 Calcein Delivery

There was no significant cell dislodgement at a flow rate of 9 mL/s (wall shear stress = 24 dyne/cm²) in the absence of ultrasound and microbubbles. No calcein uptake was observed when either ultrasound or microbubbles were applied alone. Significantly enhanced calcein delivery was observed at PNP of 200 and 300 kPa (Fig 3.5). Maximum cell delivery of 58% occurred at 200 kPa and maximum cell death of 14% at 300 kPa. Cell dislodgement was <1%, 12%, and 28% at PNP 100, 200, 300, respectively.

Maximum cell dislodgement was observed at 300 kPa. At this PNP, microbubbles were observed to aggregate on the Thermanox coverslips under flow. This may have been a consequence of secondary radiation force [85]. This would cause local microbubble concentrations to be high and thus result in greater cell dislodgement and reduced delivery. At 200

kPa there was reduced aggregation on the coverslip, and thus there was probably a more optimal microbubble-to-cell ratio resulting in reduced cell dislodgement and greater delivery. There was a clear threshold from 100 kPa to 200 kPa for delivery (Fig 3.5E), suggesting that ultrasound parameters must be optimized to enable specific spatiotemporal delivery from microbubbles generated upstream in real-time.

Cell dislodgement positively correlated with delivery, as evidenced by non-confluent patches or cellular debris after delivery. It is unknown whether the cells that dislodged were dead or successfully permeabilized, thus percent dislodgement was reported as a separate metric. Cell dislodgement is likely reduced *in vivo* as the basement membrane and collection of anchoring factors present *in vivo* are absent *in vitro*.

In practice, a tradeoff has to be made between cell viability and delivery for optimal therapeutic results. An important factor is microbubble concentration at the therapeutic site [86]. Local microbubble concentration is highly variable depending on factors such as injection site, method of administration (e.g. infusion or bolus), and transit time (i.e. distance to location of interest). By using a microfluidic platform, microbubble concentration—and thus the therapeutic efficacy—can be precisely controlled. Additionally, microbubble size and composition could be tailored for specific applications, predefined or in real-time as required. A therapeutic agent can be co-injected, as in our study, or incorporated directly in the liquid phase. Thus, a drug-modified microbubble could essentially be formed in a single step [87], without the need for an incubation/conjugation period.

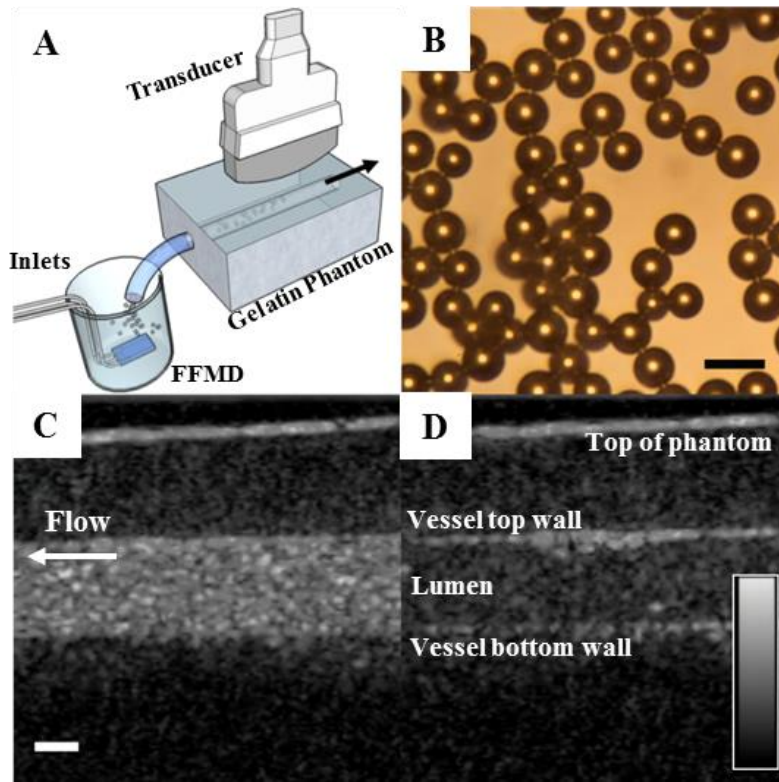


Figure 3.6: (A) Bovine blood plasma microbubbles were imaged by drawing bovine blood + microbubbles through a flow phantom. Flow direction is indicated by arrow. (B) Microbubbles immediately exiting the FFMD were monodisperse (polydispersity index < 10%) (scale bar = 20 μm). (C) Microbubbles generated in real-time produced a 6.5 dB increase in signal intensity compared to the empty vessel lumen (D). Microbubbles were destroyed by increasing the MI to 1.9. (For bottom row: scale bar = 2 mm, dynamic range scale = 100 dB, CPS gain = 0 dB).

3.3.4 Bovine Plasma Microbubbles

Production characteristics of bovine plasma microbubbles were similar to BSA microbubbles—greater than 10^5 MB/s for 10-16 μm diameter microbubbles. Blood plasma alone produced microbubbles that coalesced shortly downstream. Adding dextrose up to 40% failed to eliminate coalescence, while 2.5% GP eliminated coalescence. Microbubbles exited monodisperse (Fig 3.6B) but quickly went through Ostwald ripening, as with the BSA microbubbles, with more than 90% of microbubbles dissolved after one minute.

Plasma microbubbles enhanced contrast in blood in a gelatin flow phantom immediately after production. The microbubbles produced a 6.5 dB increase in acoustic response over the empty blood filled lumen (Fig 3.6c). At an MI of 0.2, T_i was calculated to be 3.2 ± 0.2 s. At an MI of 1.9, T_i was calculated to be 0.9 ± 0.4 s and was statistically shorter ($p < 0.0001$), indicating that increasing ultrasound pressure increased destruction (Fig 3.6D).

Microbubbles were successfully fabricated from bovine blood plasma with the addition of GP at a concentration equal to the concentration used with BSA (2.5%). The same case was not observed with dextrose, as dextrose reduced but failed to completely eliminate coalescence. While these results suggest that dissimilar mechanisms act to stabilize the microbubble shell, there are many other components (e.g. proteins, clotting factors, lipids, etc.) in blood plasma that are surface active and may have contributed to our finding. Further studies are needed to understand the mechanisms. The plasma microbubbles stabilized in GP exhibited similar production characteristics to BSA microbubbles. The microbubbles maintained monodispersity for a short duration and quickly dissolved. No insoluble aggregates were optically resolvable at 40x magnification, suggesting the shell solubilizes when the microbubbles shrink and collapse.

Traditionally microbubbles are administered on the order of $\sim 10^9$ microbubbles per patient [47], [88]; however, we found a production rate of $\sim 10^5$ MB/s provided good contrast in a flow phantom (Fig 3.6C). The microbubbles survived under flow and microbubbles within the field of view quickly dissolved when flow was halted. The plasma microbubbles were readily destroyed using a clinical scanner, demonstrating their potential for sonoporation and drug delivery. The ability for microbubbles to be fabricated from blood and dissolve on their own or be destroyed by ultrasound creates an inherently safe biocompatible agent with the

benefits of conventional monodisperse microbubbles. The short lifetime of these agents make them ideal for intravascular fabrication near the therapeutic target despite their relatively large diameter. Their lifetime may be extended by incorporating a perfluorocarbon gas . Further studies are needed to determine if parameters optimized for bovine blood are relevant to human blood, as humans have different diets as well as a different collection of surface active molecules in plasma.

By using a microfluidic device to generate plasma microbubbles, microfluidics could also be used to separate plasma from whole blood. In this study, the plasma had to be filtered out in several steps, as there are large aggregates and red blood cells that may clog the device and prohibit extended operation. Instead of bench-top centrifugation and filtration, using a microfluidic device for blood plasma separation [76], [89] potentially allows the whole process to be miniaturized and performed *in situ*. Thus, the authors envision a system (i.e. catheter) where the patient's own blood is injected and microbubbles are produced.

3.4 Conclusions

Although promising results with large ($>10\text{ }\mu\text{m}$) diameter microbubbles were demonstrated within a flow chamber, we did not do a comparison of delivery or image contrast with microbubbles under $10\text{ }\mu\text{m}$. Our lithography was limited in the smallest feature size possible, because we were limited to an aspect ratio of approximately 1:2. Thus a smaller orifice would mean a smaller microchannel height. Although it is possible to operate with smaller channel heights, there is increased fluidic resistance and thus higher pressures are needed. An alternative method of obtaining smaller microbubbles would be relying on microbubble dissolution for mixed-gas microbubbles. Such compositions will be explored in the future.

Additionally, it is not known how large transiently stable microbubbles would perform *in vivo*. There is still the question of if such microbubbles will dissolve quickly enough to prevent entrapment in vessels and how delivery and contrast will compare to *in vitro* results. Until *in vivo* studies are conducted, such questions will certainly be the focus as this project progresses.

In this chapter, we report the first case of generating albumin-coated microbubbles from fractionated BSA and blood plasma using a flow-focusing microfluidic device. Dextrose and glycerol + propylene glycol helped stabilize the albumin microbubbles generated in the FFMD. Microfluidic devices can be operated under predefined parameters at the point-of-care, decreasing the uncertainty of microbubble characteristics at the target site. By generating microbubbles *in situ*, novel microbubbles compositions can be utilized, such as large microbubbles that dissolve downstream and yet are monodisperse within proximity of the FFMD. Although the BSA microbubbles exhibited short half-lives, they persisted long enough to be imaged in blood and enhanced delivery of a model therapeutic.

Chapter 4

Discussions and Conclusions

In chapter 2, we presented the flooded method to enable microfluidic devices to be miniaturized to vascular dimensions. Thus, microfluidic devices can be potentially incorporated onto the distal end of a catheter. In chapter 3, we showed a proof of concept of real-time generation and delivery of microbubbles and a model drug with a non-flooded device. This allows controlled and specific delivery of microbubbles and drug. With the results presented in these studies, we can feasibly move towards integrating all aspects into a functional microfluidic catheter for imaging and therapeutics. Insonation can be performed with intravascular ultrasound (IVUS) (Fig 4.1) or with an external ultrasound probe.

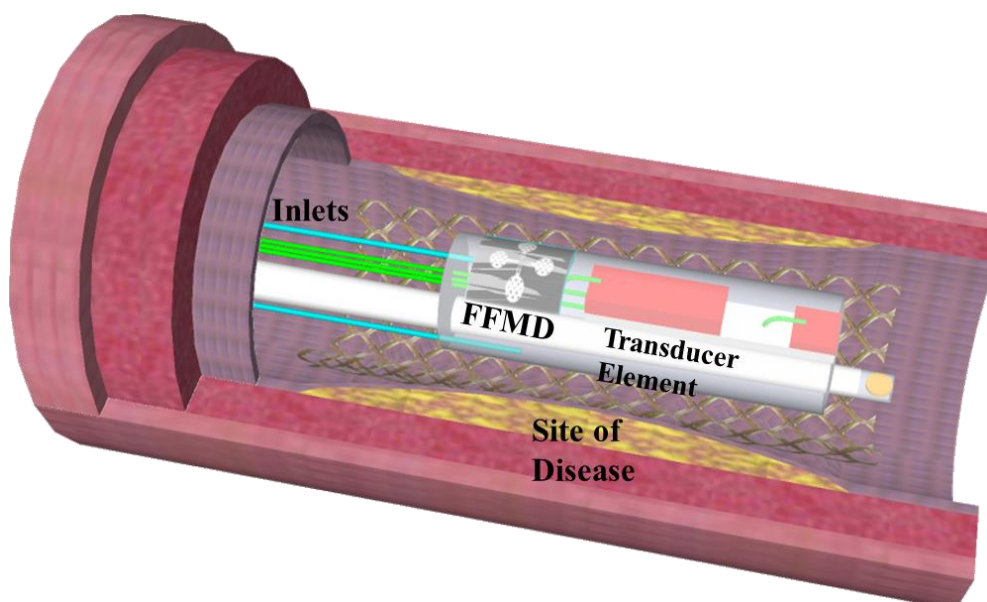


Figure 4.1: Conceptual schematic of a catheter for *in situ* production and delivery of microbubbles and therapeutics. A FFMD is upstream of an IVUS transducer element. At the site of disease, microbubbles are produced and immediately ejected near the site of disease. Microbubbles can be imaged before delivery of a therapeutic.

Alternatively, this technology may be implemented into infusion catheters to assist in uptake of cytotoxic drugs, potentially reducing the dose needed and mitigating side effects. The microfluidic technology also enables the use of a patient's own blood at the point-of-care to generate a perfectly biocompatible agent. This can be an alternative to individuals who may be allergic to traditional contrast dyes.

We take advantage of the real-time production capabilities of microfluidic devices. By using a FFMD to generate microbubbles in the vasculature, we can develop microbubble formulations more suitable for our purposes. Microfluidic devices exhibit precise control over microbubble size, production rate, and composition. More studies are needed to evaluate if control over these parameters would be beneficial clinically. However, we can imagine situations where *in vivo* blood flow may determine local microbubble concentration and require real-time adjustment of production rate for optimal delivery and minimal cell death. Also certain applications, such as sonothrombolysis, may benefit from the energy deposition of large oscillating microbubbles. Changing the composition of the gas core can be done simply by switching to a different gas cylinder, allowing for quick adjustment of microbubble lifetime. Additionally, monodisperse microbubbles can be produced to improve imaging or therapeutic performance. Although more improvements are needed before we can realize our catheter system, we present a platform technology that can potentially boost current procedures and open new routes for diagnostic and therapeutic ultrasound.

Appendix

Microbubble Detection Algorithm

A program based on the circular Hough transform (CHT) was written to measure microbubble size distribution. The algorithm was implemented into a graphical user interface, with the assistance of undergraduate Brian Shin. There were two main types of images: high speed and DSLR (Fig A.1).

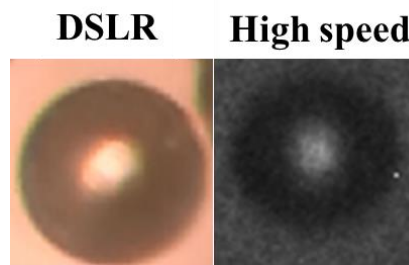


Figure A.1: Representative images of microbubbles taken with a DSLR camera and high speed camera.

Prior to CHT, the images had to be properly segmented to obtain an edgemap. Since the microbubbles have a gas core, they are optically transparent and thus appear as a clear circle with a thick dark band around it (Fig A.1). The inner circle plus the thick band comprise the whole microbubble. The images from the high speed camera were noisier than the optical images taken with the DSLR. Thus, the high speed images were median filtered (square 10x10 window) to get rid of the speckle-like noise. The images from the DSLR had bright/dark regions (originating from the misalignment of the experimental lighting), causing

low contrast in regions where lighting was darker. Adaptive histogram equalization was used to correct this and provide steady contrast for the whole image. After these corrections were made to the respective images, the images were binarized using Otsu's method to find the appropriate threshold level (Fig A.2A). Connected component analysis was used to detect the thick band of the microbubbles (Fig A.2B) and the centers of the microbubbles (Fig A.2C). These two images were added to form a whole circle representing the microbubble (Fig A.2D). This image was then used to form the edge map (Fig A.2E).

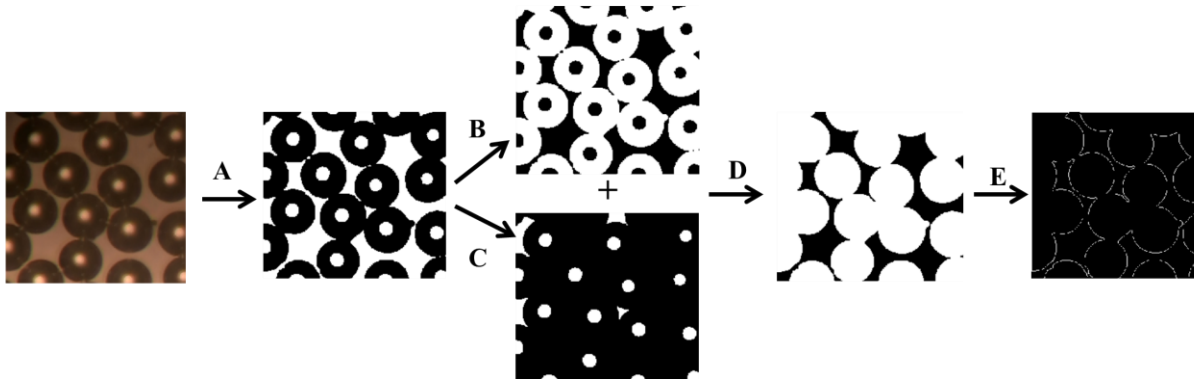


Figure A.2: Flow chart for obtaining the edge map to pass to the CHT. (A) Original image was put through adaptive histogram equalization and thresholded using Otsu's method for finding a threshold level. (B) The microbubble band and (C) the microbubble center was detected using connected components, specifying an acceptable range of pixel areas and excluding all other areas that fall outside the range. (D) The results from (B) and (C) were added to form a whole microbubble. (E) The edge map was created.

The edge map was passed through a circular Hough transform to detect the circular MBs. For images of stationary microbubbles taken with a DSLR, the CHT detected greater than 95% of the MBs (Fig A.3A). The mean microbubble diameter agreed well (error < 6%) and the PDI were nearly identical (error < 2%) compared with manual measurements. For high speed images where microbubbles were moving, the CHT detected MBs that were circular but failed to detect the non-circular microbubbles (Fig A.3B). The measured mean diameter and polydispersity index were in close agreement as well. For images where production rate was high, and thus there were many microbubbles in close proximity to each other, detec-

tion was much more difficult because most of the microbubbles were deformed to a non-circular shape (Fig A.3C). The CHT resulted in false detection of ellipsoid-shaped microbubbles. A possible solution would be to parameterize an ellipsoid and implement the Hough transform for ellipsoid- microbubbles. This method would require the user to specify which transform to use or to develop a way to trigger the right transform (circular or ellipsoid) based on the current image.

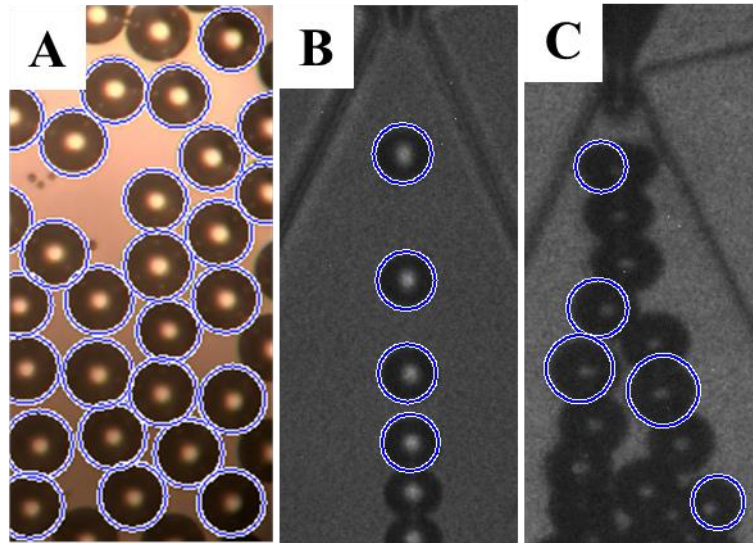


Figure A.3: CHT processed images. (A) DSLR image showing good detection. (B) High speed image showing detection of isolated circulated microbubbles. (C) High speed image showing poor detection due to microbubbles crowding.

%% Code for microbubble detection

%% Load, filter, and binarize image

```
I=imread('Bubble.jpg'); % Load microbubble image
```

% Convert to grayscale and median filter or adaptive histogram

```
I2 = rgb2gray(I);
I2 = medfilt2(I2, [5 5]);
% I2 = adapthisteq(I2);
```

% Otsu's method to threshold

```
level = graythresh(I2);
BW = im2bw(I2,level);
```

```
imshow(BW)
```

%% Use connected components to isolate the centers of bubbles

% Connected component labeling

```
labeledImage = bwlabel(BW, 8);
blobprop = regionprops(labeledImage, I2, 'all');
numBlobs = size(blobprop, 1);
BGfill = BW;
```

% Exclude regions that are not microbubble centers

```
for n = 1:numBlobs
    if(blobprop(n).Area > 1500 | blobprop(n).Area < 100)
        for i = 1:blobprop(n).Area
            BGfill(blobprop(n).PixelList(i,2),blobprop(n).PixelList(i,1))=0;
        end
    end
end
```

```
figure
imshow(BGfill)
title('Fill everything except centers')
```

%% Obtain binary image of filled bubbles without centers

% Add thick layer + microbubble center

```
MBfill = imcomplement(BW)+BGfill;
imshow(MBfill)
% Connected component labeling
labeledImage = bwlabel(MBfill, 8);
blobprop = regionprops(labeledImage,I2,'all');
numBlobs = size(blobprop, 1);
```

% Exclude regions that are too small to be bubbles

```
for n = 1:numBlobs
    if(blobprop(n).Area < 4400)
        for i = 1:blobprop(n).Area
            MBfill(blobprop(n).PixelList(i,2),blobprop(n).PixelList(i,1))=0;
        end
    end
end
end
```

```
figure
imshow(MBfill)
title('Filled MBs')
```

%% obtain edge map

```
edge = imopen(MBfill, ones(5,5));
edge = bwareaopen(edge, 40);
perim = bwperim(edge);
figure
imshow(perim)
title('Edge map')
```

%% Perform circle hough transform and plot distribution, refer to matlab

%% help file on the imfindcircles

radii = [30 90]; % Radii range in pixels

```
[centers, radii, metric] = imfindcircles(perim,radii, 'Sensitivity', .95);
```

```
figure
imshow(I)
hold on
viscircles(centers, radii,'EdgeColor','b');
count = length(centers(:,1));
title(['number of bubbles =', num2str(count)]);
```

scale = 5.4 % units = pixels/um

real_diam = radii.*2/scale; %Convert to um units

```
figure
hist(real_diam,20)
diam_mean = mean(real_diam);
diam_stdev=std(real_diam);
```

```
title(['mean =', num2str(diam_mean),' stdev =', num2str(diam_stdev)]);
```

References

- [1] G. M. Campbell and E. Mougeot, "Creation and characterisation of aerated food products," *Trends in Food Science & Technology*, vol. 10, no. 9, pp. 283–296, Sep. 1999.
- [2] T. Nishikawa, A. Yoshida, A. Khanal, M. Habu, I. Yoshioka, K. Toyoshima, T. Takehara, T. Nishihara, K. Tachibana, and K. Tominaga, "A study of the efficacy of ultrasonic waves in removing biofilms," *Gerodontology*, vol. 27, no. 3, pp. 199–206, Sep. 2010.
- [3] A. Agarwal, W. J. Ng, and Y. Liu, "Principle and applications of microbubble and nanobubble technology for water treatment," *Chemosphere*, vol. 84, no. 9, pp. 1175–1180, Aug. 2011.
- [4] N. S. Chahal and R. Senior, "Clinical Applications of Left Ventricular Opacification," *J Am Coll Cardiol Img.*, vol. 3, no. 2, pp. 188–196, Feb. 2010.
- [5] R. Gessner and P. A. Dayton, "Advances in molecular imaging with ultrasound," *Molecular imaging*, vol. 9, no. 3, pp. 117–127, Jun. 2010.
- [6] K. Ferrara, R. Pollard, and M. Borden, "Ultrasound Microbubble Contrast Agents: Fundamentals and Application to Gene and Drug Delivery," *Annual Review of Biomedical Engineering*, vol. 9, no. 1, pp. 415–447, 2007.
- [7] W. C. Culp, R. Flores, A. T. Brown, J. D. Lowery, P. K. Roberson, L. J. Hennings, S. D. Woods, J. H. Hatton, B. C. Culp, R. D. Skinner, and M. J. Borrelli, "Successful Microbubble Sonothrombolysis Without Tissue-Type Plasminogen Activator in a Rabbit Model of Acute Ischemic Stroke," *Stroke*, vol. 42, no. 8, pp. 2280–2285, Aug. 2011.
- [8] E. Talu, K. Hettiarachchi, R. L. Powell, A. P. Lee, P. A. Dayton, and M. L. Longo, "Maintaining Monodispersity in a Microbubble Population Formed by Flow-Focusing," *Langmuir*, vol. 24, no. 5, pp. 1745–1749, Jan. 2008.
- [9] A. Myrset, H. Nicolaysen, K. Toft, C. Christiansen, and T. Skotland, "Structure and organization of albumin molecules forming the shell of air-filled microspheres: evidence for a monolayer of albumin molecules of multiple orientations stabilizing the enclosed air," *Biotechnology and Applied Biochemistry*, vol. 24, no. 2, pp. 145–153, Oct. 1996.
- [10] M. W. Grinstaff and K. S. Suslick, "Air-filled proteinaceous microbubbles: synthesis of an echo-contrast agent," *PNAS*, vol. 88, no. 17, pp. 7708–7710, Sep. 1991.
- [11] M. Wong and K. S. Suslick, "Sonochemically produced hemoglobin microbubbles," in *Materials Research Society Symposium Proceedings*, 1995, vol. 372, pp. 89–89.

- [12] E. Stride and M. Edirisinghe, "Novel preparation techniques for controlling microbubble uniformity: a comparison," *Med Biol Eng Comput*, vol. 47, no. 8, pp. 883–892, Aug. 2009.
- [13] S. Sirsi and M. Borden, "Microbubble Compositions, Properties and Biomedical Applications," *Bubble Sci Eng Technol*, vol. 1, no. 1–2, pp. 3–17, Nov. 2009.
- [14] S. H. Bloch, M. Wan, P. A. Dayton, and K. W. Ferrara, "Optical observation of lipid- and polymer-shelled ultrasound microbubble contrast agents," *Applied Physics Letters*, vol. 84, no. 4, pp. 631–633, Jan. 2004.
- [15] P. Narayan and M. A. Wheatley, "Preparation and characterization of hollow microcapsules for use as ultrasound contrast agents," *Polym Eng Sci*, vol. 39, no. 11, pp. 2242–2255, Nov. 1999.
- [16] F. S. Villanueva, E. Lu, S. Bowry, S. Kilic, E. Tom, J. Wang, J. Gretton, J. J. Pacella, and W. R. Wagner, "Myocardial ischemic memory imaging with molecular echocardiography," *Circulation*, vol. 115, no. 3, pp. 345–352, 2007.
- [17] A. Kheirrolomoom, P. A. Dayton, A. F. H. Lum, E. Little, E. E. Paoli, H. Zheng, and K. W. Ferrara, "Acoustically-active microbubbles conjugated to liposomes: characterization of a proposed drug delivery vehicle," *Journal of Controlled Release*, vol. 118, no. 3, pp. 275–284, Apr. 2007.
- [18] E. C. Unger, T. McCreery, R. Sweitzer, V. E. Caldwell, and Y. Wu, "Acoustically Active Lipospheres Containing Paclitaxel: A New Therapeutic Ultrasound Contrast Agent," *Investigative Radiology*, vol. 33, no. 12, 1998.
- [19] S. Kvåle, H. A. Jakobsen, O. A. Asbjørnsen, and T. Omtveit, "Size fractionation of gas-filled microspheres by flotation," *Separations Technology*, vol. 6, no. 4, pp. 219–226, Oct. 1996.
- [20] J. A. Feshitan, C. C. Chen, J. J. Kwan, and M. A. Borden, "Microbubble size isolation by differential centrifugation," *Journal of Colloid and Interface Science*, vol. 329, no. 2, pp. 316–324, Jan. 2009.
- [21] K. E. Morgan, J. S. Allen, P. A. Dayton, J. E. Chomas, A. L. Klibaov, and K. W. Ferrara, "Experimental and theoretical evaluation of microbubble behavior: effect of transmitted phase and bubble size," *Ultrasonics, Ferroelectrics and Frequency Control, IEEE Transactions on*, vol. 47, no. 6, pp. 1494–1509, Nov. 2000.
- [22] M. Kaya, S. Feingold, K. Hettiarachchi, A. P. Lee, and P. A. Dayton, "Acoustic responses of monodisperse lipid encapsulated microbubble contrast agents produced by flow focusing," *Bubble Science, Engineering & Technology*, vol. 2, no. 2, pp. 33–40, 2010.
- [23] E. Talu, K. Hettiarachchi, S. Zhao, R. L. Powell, A. P. Lee, M. L. Longo, and P. A. Dayton, "Tailoring the size distribution of ultrasound contrast agents: possible method for

- improving sensitivity in molecular imaging,” *Molecular imaging*, vol. 6, no. 6, pp. 384–392, 2007.
- [24] Y. Gong, M. Cabodi, and T. Porter, “Relationship between size and frequency dependent attenuation of monodisperse populations of lipid coated microbubbles,” *Bubble Science, Engineering & Technology*, vol. 2, no. 2, pp. 41–47, 2010.
- [25] J. J. Choi, J. A. Feshitan, B. Baseri, S. Wang, Y.-S. Tung, M. A. Borden, and E. E. Konofagou, “Microbubble-Size Dependence of Focused Ultrasound-Induced Blood-Brain Barrier Opening in Mice In Vivo,” *IEEE Transactions on Biomedical Engineering*, vol. 57, no. 1, pp. 145–154, Jan. 2010.
- [26] Z. Fan, H. Liu, M. Mayer, and C. X. Deng, “Spatiotemporally controlled single cell sonoporation,” *PNAS*, Sep. 2012.
- [27] C. Zhang, J. Xu, W. Ma, and W. Zheng, “PCR microfluidic devices for DNA amplification,” *Biotechnology advances*, vol. 24, no. 3, pp. 243–284, 2006.
- [28] C. Situma, M. Hashimoto, and S. A. Soper, “Merging microfluidics with microarray-based bioassays,” *Biomolecular engineering*, vol. 23, no. 5, pp. 213–231, 2006.
- [29] D. Huh, B. D. Matthews, A. Mammoto, M. Montoya-Zavala, H. Y. Hsin, and D. E. Ingber, “Reconstituting organ-level lung functions on a chip,” *Science*, vol. 328, no. 5986, pp. 1662–1668, 2010.
- [30] D. R. Link, S. L. Anna, D. A. Weitz, and H. A. Stone, “Geometrically mediated breakup of drops in microfluidic devices,” *Physical Review Letters*, vol. 92, no. 5, p. 054503, 2004.
- [31] P. Garstecki, M. J. Fuerstman, H. A. Stone, and G. M. Whitesides, “Formation of droplets and bubbles in a microfluidic T-junction—scaling and mechanism of break-up,” *Lab Chip*, vol. 6, no. 3, pp. 437–446, Feb. 2006.
- [32] A. M. Gañán-Calvo and J. M. Gordillo, “Perfectly monodisperse microbubbling by capillary flow focusing,” *Phys. Rev. Lett*, vol. 87, no. 27 Pt 1, p. 274501, Dec. 2001.
- [33] U. Farook, H. B. Zhang, M. J. Edirisinghe, E. Stride, and N. Saffari, “Preparation of microbubble suspensions by co-axial electrohydrodynamic atomization,” *Med Eng Phys*, vol. 29, no. 7, pp. 749–754, Sep. 2007.
- [34] J. M. Gordillo, Z. Cheng, A. M. Ganan-Calvo, M. Márquez, and D. A. Weitz, “A new device for the generation of microbubbles,” *Phys. Fluids*, vol. 16, no. 8, p. 2828, 2004.
- [35] P. Garstecki, I. Gitlin, W. DiLuzio, G. M. Whitesides, E. Kumacheva, and H. A. Stone, “Formation of monodisperse bubbles in a microfluidic flow-focusing device,” *Appl. Phys. Lett.*, vol. 85, no. 13, pp. 2649–2651, Sep. 2004.

- [36] E. Talu, M. M. Lozano, R. L. Powell, P. A. Dayton, and M. L. Longo, "Long-term stability by lipid coating monodisperse microbubbles formed by a flow-focusing device," *Langmuir*, vol. 22, no. 23, pp. 9487–9490, Nov. 2006.
- [37] K. Hettiarachchi, E. Talu, M. L. Longo, P. A. Dayton, and A. P. Lee, "On-chip generation of microbubbles as a practical technology for manufacturing contrast agents for ultrasonic imaging," *Lab Chip*, vol. 7, no. 4, pp. 463–468, Apr. 2007.
- [38] T. Cubaud, M. Tatineni, X. Zhong, and C.-M. Ho, "Bubble dispenser in microfluidic devices," *Phys Rev E Stat Nonlin Soft Matter Phys*, vol. 72, no. 3 Pt 2, p. 037302, Sep. 2005.
- [39] E. Castro-Hernández, W. van Hoeve, D. Lohse, and J. M. Gordillo, "Microbubble generation in a co-flow device operated in a new regime," *Lab Chip*, vol. 11, no. 12, pp. 2023–2029, Jun. 2011.
- [40] D. C. Duffy, J. C. McDonald, O. J. Schueller, and G. M. Whitesides, "Rapid Prototyping of Microfluidic Systems in Poly(dimethylsiloxane)," *Anal. Chem.*, vol. 70, no. 23, pp. 4974–4984, Dec. 1998.
- [41] J. C. McDonald, D. C. Duffy, J. R. Anderson, D. T. Chiu, H. Wu, O. J. Schueller, and G. M. Whitesides, "Fabrication of microfluidic systems in poly(dimethylsiloxane)," *Electrophoresis*, vol. 21, no. 1, pp. 27–40, Jan. 2000.
- [42] J. R. Hung and L. Lin, "Micro-to-macro fluidic interconnectors with an integrated polymer sealant," *Journal of Micromechanics and Microengineering*, vol. 11, no. 5, pp. 577–581, Sep. 2001.
- [43] A. M. Christensen, D. A. Chang-Yen, and B. K. Gale, "Characterization of interconnects used in PDMS microfluidic systems," *Journal of Micromechanics and Microengineering*, vol. 15, no. 5, p. 928, 2005.
- [44] K. D. Daniel, G. Y. Kim, C. C. Vassiliou, F. Jalali-Yazdi, R. Langer, and M. J. Cima, "Multi-reservoir device for detecting a soluble cancer biomarker," *Lab on a Chip*, vol. 7, no. 10, pp. 1288–1293, 2007.
- [45] C. Foley, N. Nishimura, K. Neeves, C. Schaffer, and W. Olbricht, "Flexible microfluidic devices supported by biodegradable insertion scaffolds for convection-enhanced neural drug delivery," *Biomed Microdevices*, vol. 11, no. 4, pp. 915–924, Aug. 2009.
- [46] C. C. Chen and M. A. Borden, "Ligand Conjugation to Bimodal Poly(ethylene glycol) Brush Layers on Microbubbles," *Langmuir*, vol. 26, no. 16, pp. 13183–13194, Jul. 2010.
- [47] "Optison (Package Insert)." Little Chalfont, UK: GE Healthcare, 2000.
- [48] E. Talu, R. L. Powell, M. L. Longo, and P. A. Dayton, "Needle size and injection rate impact microbubble contrast agent population," pp. 1182–1185, Jul. 2008.

- [49] B. D. Butler and B. A. Hills, "The lung as a filter for microbubbles," *J Appl Physiol*, vol. 47, no. 3, pp. 537–543, Sep. 1979.
- [50] H. Iijima, F. Moriyasu, T. Miyahara, and K. Yanagisawa, "Ultrasound contrast agent, Levovist microbubbles are phagocytosed by Kupffer cells—In vitro and in vivo studies," *Hepatology Research*, vol. 35, no. 4, pp. 235–237, Aug. 2006.
- [51] A. K. P. Lim, N. Patel, R. J. Eckersley, S. D. Taylor-Robinson, D. O. Cosgrove, and M. J. K. Blomley, "Evidence for spleen-specific uptake of a microbubble contrast agent: a quantitative study in healthy volunteers," *Radiology*, vol. 231, no. 3, pp. 785–788, Jun. 2004.
- [52] V. Barbier, H. Willaime, P. Tabeling, and F. Jousse, "Producing droplets in parallel microfluidic systems," *Phys. Rev. E*, vol. 74, no. 4, p. 046306, Oct. 2006.
- [53] K. Hettiarachchi, E. Talu, M. L. Longo, P. A. Dayton, and A. P. Lee, "Multi-Array Flow-Focusing Devices to Accelerate Production of Microbubbles for Contrast-Enhanced Ultrasound Imaging," in *Eleventh International Conference on Miniaturized Systems for Chemistry and Life Sciences*, Paris, France, 2007, pp. 664–666.
- [54] M. Hashimoto, S. S. Shevkoplyas, B. Zasońska, T. Szymborski, P. Garstecki, and G. M. Whitesides, "Formation of bubbles and droplets in parallel, coupled flow-focusing geometries," *Small*, vol. 4, no. 10, pp. 1795–1805, Oct. 2008.
- [55] W. Li, E. W. K. Young, M. Seo, Z. Nie, P. Garstecki, C. A. Simmons, and E. Kumacheva, "Simultaneous generation of droplets with different dimensions in parallel integrated microfluidic droplet generators," *Soft Matter*, vol. 4, no. 2, pp. 258–262, Jan. 2008.
- [56] M. K. Mulligan and J. P. Rothstein, "Scale-up and control of droplet production in coupled microfluidic flow-focusing geometries," *Microfluid. Nanofluid.*, vol. 13, no. 1, pp. 65–73, Jul. 2012.
- [57] J. C. Love, J. R. Anderson, and G. M. Whitesides, "Fabrication of three-dimensional microfluidic systems by soft lithography," *MRS Bull.*, vol. 26, no. 7, pp. 523–528, Jul. 2001.
- [58] C. Jiang, X. Li, F. Yan, Z. Wang, Q. Jin, F. Cai, M. Qian, X. Liu, L. Zhang, and H. Zheng, "Microfluidic-assisted formation of multifunctional monodisperse microbubbles for diagnostics and therapeutics," *Micro Nano Lett.*, vol. 6, no. 6, pp. 417–421, Jun. 2011.
- [59] M.-E. Vlachopoulou, A. Tserepi, P. Pavli, P. Argitis, M. Sanopoulou, and K. Misiakos, "A low temperature surface modification assisted method for bonding plastic substrates," *J. Micromech. Microeng.*, vol. 19, no. 1, p. 015007, Jan. 2009.
- [60] P. Guillot and A. Colin, "Stability of parallel flows in a microchannel after a T junction," *Phys. Rev. E*, vol. 72, no. 6, p. 066301, Dec. 2005.

- [61] J. H. Xu, S. W. Li, Y. J. Wang, and G. S. Luo, "Controllable gas-liquid phase flow patterns and monodisperse microbubbles in a microfluidic T-junction device," *Appl. Phys. Lett.*, vol. 88, no. 13, Mar. 2006.
- [62] K. Hettiarachchi and A. P. Lee, "Polymer-lipid microbubbles for biosensing and the formation of porous structures," *Journal of Colloid and Interface Science*, vol. 344, no. 2, pp. 521–527, Apr. 2010.
- [63] M. W. Keller, W. Glasheen, and S. Kaul, "Albunex: a safe and effective commercially produced agent for myocardial contrast echocardiography," *Journal of the American Society of Echocardiography: official publication of the American Society of Echocardiography*, vol. 2, no. 1, pp. 48–52, Feb. 1989.
- [64] R. P. Garvin, M. J. Duryee, L. W. Klassen, G. M. Thiele, and D. R. Anderson, "Ultrasound Imaging in an Animal Model of Vascular Inflammation Following Balloon Injury," *Ultrasound in Medicine & Biology*, vol. 38, no. 9, pp. 1552–1558, Sep. 2012.
- [65] G. Korpanty, P. A. Grayburn, R. V. Shohet, and R. A. Brekken, "Targeting vascular endothelium with avidin microbubbles," *Ultrasound in Medicine & Biology*, vol. 31, no. 9, pp. 1279–1283, Sep. 2005.
- [66] R. J. Browning, H. Mulvana, M.-X. Tang, J. V. Hajnal, D. J. Wells, and R. J. Eckersley, "Effect of Albumin and Dextrose Concentration on Ultrasound and Microbubble Mediated Gene Transfection In Vivo," *Ultrasound in Medicine & Biology*, vol. 38, no. 6, pp. 1067–1077, Jun. 2012.
- [67] M. Duvshani-Eshet, D. Adam, and M. Machluf, "The effects of albumin-coated microbubbles in DNA delivery mediated by therapeutic ultrasound," *Journal of Controlled Release*, vol. 112, no. 2, pp. 156–166, May 2006.
- [68] P. A. Frenkel, S. Chen, T. Thai, R. V. Shohet, and P. A. Grayburn, "Dna-loaded albumin microbubbles enhance ultrasound-mediated transfection in vitro," *Ultrasound in Medicine & Biology*, vol. 28, no. 6, pp. 817–822, Jun. 2002.
- [69] K. Tachibana and S. Tachibana, "Albumin Microbubble Echo-Contrast Material as an Enhancer for Ultrasound Accelerated Thrombolysis," *Circulation*, vol. 92, no. 5, pp. 1148–1150, Sep. 1995.
- [70] S. Podell, C. Burrascano, M. Gaal, B. Golec, J. Maniquis, and P. Mehlhaff, "Physical and biochemical stability of Optison®, an injectable ultrasound contrast agent," *Biotechnology and Applied Biochemistry*, vol. 30, no. 3, pp. 213–223, 1999.
- [71] J.-L. Vincent, M. M. Wilkes, and R. J. Navickis, "Safety of human albumin—serious adverse events reported worldwide in 1998–2000†," *Br. J. Anaesth.*, vol. 91, no. 5, pp. 625–630, Nov. 2003.
- [72] L. Dalla Palma and M. Bertolotto, "Introduction to ultrasound contrast agents: physics overview," *European Radiology*, vol. 9, no. S3, pp. S338–S342, Nov. 1999.

- [73] J. M. Gorce, M. Arditi, and M. Schneider, "Influence of bubble size distribution on the echogenicity of ultrasound contrast agents: a study of SonoVue," *Invest Radiol*, vol. 35, no. 11, pp. 661–671, Nov. 2000.
- [74] A. Krishnan, J. Sturgeon, C. A. Siedlecki, and E. A. Vogler, "Scaled interfacial activity of proteins at the liquid–vapor interface," *Journal of Biomedical Materials Research Part A*, vol. 68A, no. 3, pp. 544–557, 2004.
- [75] S. Avivi and A. Gedanken, "S-S bonds are not required for the sonochemical formation of proteinaceous microspheres: the case of streptavidin.," *Biochem J*, vol. 366, no. 3, pp. 705–707, Sep. 2002.
- [76] S. Yang, A. Undar, and J. D. Zahn, "A microfluidic device for continuous, real time blood plasma separation," *Yang, Sung, Akif Ündar, and Jeffrey D. Zahn. "A microfluidic device for continuous, real time blood plasma separation." Lab on a Chip 6, no. 7 (2006): 871-880.*, vol. 6, no. 7, p. 871, 2006.
- [77] D. H. Ballard, "Generalizing the Hough transform to detect arbitrary shapes," *Pattern Recognition*, vol. 13, no. 2, pp. 111–122, 1981.
- [78] N. de Jong, A. Bouakaz, and P. Frinking, "Basic acoustic properties of microbubbles," pp. 229–240, Apr. 2002.
- [79] T. Sanada, M. Watanabe, and T. Fukano, "Effects of viscosity on coalescence of a bubble upon impact with a free surface," *Chemical Engineering Science*, vol. 60, no. 19, pp. 5372–5384, Sep. 2005.
- [80] L. Chen, Y. Li, and R. Manasseh, "The coalescence of bubbles-A numerical study," presented at the Third International Conference on Multiphase Flow, ICMF, 1998, vol. 98, pp. 8–12.
- [81] E. Talu, K. Hettiarachchi, H. Nguyen, A. P. Lee, R. L. Powell, M. L. Longo, and P. A. Dayton, "P2A-8 Lipid-Stabilized Monodisperse Microbubbles Produced by Flow Focusing for Use as Ultrasound Contrast Agents," in *IEEE Ultrasonics Symposium, 2006*, 2006, pp. 1568 –1571.
- [82] T. Porter, F. Xie, J. Anderson, A. Kricsfeld, and A. D'Sa, "Multifold sonicated dilutions of albumin with fifty percent dextrose improve left ventricular contrast videointensity after intravenous injection in human beings.," *J Am Soc Echocardiogr*, vol. 7, no. 5, pp. 465–471, 1994.
- [83] H. Hellebust, C. Christiansen, and T. Skotland, "Biochemical characterization of air-filled albumin microspheres," *Biotechnology and Applied Biochemistry*, vol. 18, no. 3, pp. 227–237, 1993.
- [84] G. Maltezos, M. Johnston, and A. Scherer, "Thermal management in microfluidics using micro-Peltier junctions," *Applied Physics Letters*, vol. 87, no. 15, pp. 154105 – 154105–3, Oct. 2005.

- [85] P. Dayton, A. Klibanov, G. Brandenburger, and K. Ferrara, "Acoustic radiation force in vivo: a mechanism to assist targeting of microbubbles," *Ultrasound in Medicine & Biology*, vol. 25, no. 8, pp. 1195–1201, Oct. 1999.
- [86] A. Rahim, S. L. Taylor, N. L. Bush, G. R. ter Haar, J. C. Bamber, and C. D. Porter, "Physical parameters affecting ultrasound/microbubble-mediated gene delivery efficiency in vitro," *Ultrasound in medicine & biology*, vol. 32, no. 8, pp. 1269–1279, Aug. 2006.
- [87] S. A. Peyman, R. H. Abou-Saleh, J. R. McLaughlan, N. Ingram, B. R. G. Johnson, K. Critchley, S. Freear, J. A. Evans, A. F. Markham, P. L. Coletta, and S. D. Evans, "Expanding 3D geometry for enhanced on-chip microbubble production and single step formation of liposome modified microbubbles," *Lab Chip*, vol. 12, no. 21, pp. 4544–4552, 2012.
- [88] "Definity (Package Insert)." North Billerica, MA: Lantheus Medical Imaging, 2008.
- [89] T. Crowley and V. Pizziconi, "Isolation of plasma from whole blood using planar microfilters for lab-on-a-chip applications," *Lab on a Chip*, vol. 5, no. 9, p. 922, 2005.